DOI: 10.1002/chem.200800856

Combination of Lacunary Polyoxometalates and High-Nuclear Transition Metal Clusters under Hydrothermal Conditions: IX. A Series of Novel Polyoxotungstates Sandwiched by Octa-Copper Clusters

Jun-Wei Zhao,[a] Chun-Mei Wang,[a, b] Jie Zhang,[a] Shou-Tian Zheng,[a] and Guo-Yu Yang*[a]

Abstract: The reaction of $CuCl_2{\cdot}2H_2O$ with trivacant Keggin polyoxoanions $K_8Na_2[A\text{-}\alpha\text{-}GeW_9O_{34}]{\cdot}25H_2O$ or $K_{10}[A\text{-}\alpha\text{-}SiW_9O_{34}]{\cdot}25H_2O$ in the presence of 1,2-diaminopropane (dap), ethylenediamine (en) or 2,2′-bipyridine (2,2′-bpy) under hydrothermal conditions afforded five novel hybrid inorganic–organic octa-Cu sandwiched polyoxotungstates (POTs): $H_4[Cu^{II}_8(dap)_4(H_2O)_2(B\text{-}\alpha\text{-}GeW_9O_{34})_2]{\cdot}13H_2O$ (**1**), $(H_2en)_2[Cu^{II}_8(en)_4(H_2O)_2(B\text{-}\alpha\text{-}GeW_9O_{34})_2]{\cdot}5H_2O$(**2**), $(H_2en)_2[Cu^{II}_8(en)_4(H_2O)_2(B\text{-}\alpha\text{-}SiW_9O_{34})_2]{\cdot}8H_2O$ (**3**), $[Cu^{II}(H_2O)_2]H_2[Cu^{II}_8(en)_4(H_2O)_2(B\text{-}\alpha\text{-}SiW_9O_{34})_2]$ (**4**), and $[Cu^{II}_2(H_2O)_2(2,2'\text{-}bpy)_2]\{[Cu^{II}(bdyl)]_2[Cu^{II}_8(2,2'\text{-}bpy)_4(H_2O)_2(B\text{-}\alpha\text{-}GeW_9O_{34})_2]\}{\cdot}4H_2O$ (bdyl = 2,2′-bipyridinyl)(**5**). Additionally, $CuCl_2{\cdot}2H_2O$ reacts with the mixture of GeO_2, $Na_2WO_4{\cdot}2H_2O$, $H_2SiW_{12}O_{40}{\cdot}2H_2O$ in the presence of 2,2′-bpy and 4,4′-bpy under hydrothermal conditions leading to another novel mixed-valent octa-Cu sandwiched POT hybrid: $[Cu^{I}(2,2'\text{-}bpy)(4,4'\text{-}bpy)]_2[\{Cu^{I}_2(2,2'\text{-}bpy)_2(4,4'\text{-}bpy)\}_2[Cu^{I}_2Cu^{II}_6(2,2'\text{-}bpy)_2(4,4'\text{-}bpy)_2(B\text{-}\alpha\text{-}GeW_9O_{34})_2]]{\cdot}2H_2O$ (**6**). **1**, **2**, and **3** are discrete dimers constructed from two trivacant Keggin $[B\text{-}\alpha\text{-}XW_9O_{34}]^{10-}$ ($X = Ge^{IV}/Si^{IV}$) fragments and an octa-Cu cluster whereas **4** displays the 3D (3,6)-connected nets with $(4{\cdot}6^2)(4^2{\cdot}6^4{\cdot}8^7{\cdot}10^2)$ topology, which are built by octa-Cu sandwiched polyoxometalate building blocks through copper cation bridges. **5** is a novel 2D layer based on octa-Cu sandwiched POT clusters and $[Cu^{II}_2(bdyl)]$ units. Interestingly, the rollover metalation of 2,2′-bpy is firstly observed in the system containing the copper complex under hydrothermal conditions. **6** is a discrete mixed-valent octa-Cu sandwiched POT supported by two Cu^{I}-complexes $[Cu^{I}_2(2,2'\text{-}bpy)_2(4,4'\text{-}bpy)]^{2+}$ through 4,4′-bpy bridges, which constructs a novel dodeca-copper cluster. Notably, the octa-Cu cluster in **6** is mixed-valent and is different from those in **1**–**5**. To our knowledge, **1**–**6** represent a rare family of POTs incorporating novel octa-nuclear transition-metal clusters in polyoxometalate chemistry. They were structurally characterized by FT-IR spectra, elemental analysis, thermogravimetric analysis, and single-crystal X-ray diffraction. The magnetic properties of **1**, **4**, and **5** were quantitatively analyzed by the MAGPACK software package.

Keywords: copper · keggin structure · metal-oxo cluster · octanuclear copper · polyoxometalates

Introduction

Polyoxometalates (POMs) have been attracting extensive interest in solid-state material chemistry in the past several decades, not only because of enormous compositional and electronic tenability, the unique topologies, but also the wide range of potential applications in medicine, catalysis, analytical chemistry, electrochromism, and magnetism.[1] Since the occurrence of a multitude of lacunary polyoxoanions derived from Keggin-type $[XW_{12}O_{40}]^{n-}$ ($X = P^V/As^V/Si^{IV}/Ge^{IV}$) and Dawson-type $[\alpha\text{-}X_2W_{18}O_{62}]^{6-}$ ($X = P^V/As^V$) polyoxoanions, the discovery and investigation of their lacunary derivatives, such as phosphotungstates, silicotungstates, and germanotungstates, has been a significant focus in POM

[a] J.-W. Zhao, Dr. C.-M. Wang, Prof. Dr. J. Zhang, S.-T. Zheng, Prof. Dr. G.-Y. Yang
State Key Laboratory of Structural Chemistry
Fujian Institute of Research on the Structure of Matter
and Graduate School of the Chinese Academy of Sciences
Fuzhou, Fujian 350002 (China)
Fax: (+86)591-83710051
E-mail: ygy@fjirsm.ac.cn

[b] Dr. C.-M. Wang
College of Chemistry and Chemical Engineering
Harbin Normal University
Harbin, Heilongjiang 150080 (China)

Supporting information for this article is available on the WWW under http://dx.doi.org/10.1002/chem.200800856.

chemistry.[2] It is well known that monovacant ($[\alpha\text{-}PW_{11}O_{39}]^{7-}$, $[\alpha\text{-}SiW_{11}O_{39}]^{8-}$, $[\alpha\text{-}GeW_{11}O_{39}]^{8-}$ or $[\alpha\text{-}P_2W_{17}O_{61}]^{10-}$),[3a] divacant ($[\gamma\text{-}PW_{10}O_{36}]^{7-}$, $[\gamma\text{-}SiW_{10}O_{36}]^{8-}$ or $[\gamma\text{-}GeW_{10}O_{36}]^{8-}$),[3b–d] trivacant ($[\alpha\text{-}PW_9O_{34}]^{9-}$, $[\alpha\text{-}SiW_9O_{34}]^{10-}$, $[\alpha\text{-}GeW_9O_{34}]^{10-}$ or $[\alpha\text{-}P_2W_{15}O_{56}]^{12-}$),[3e–g] and polyvacant ($[\alpha\text{-}H_2P_2W_{12}O_{48}]^{12-}$, $[H_7P_8W_{48}O_{184}]^{33-}$)[3h–i] precursors can be easily prepared in one- or two-step processes in high yields, which provide us abundant initial materials to search and exploit their derivatives under hydrothermal conditions. More importantly, these lacunary fragments can work as multidentate inorganic ligands and incorporate in situ formed transition-metal (TM) clusters, generating a rapidly growing class of transition-metal substituted polyoxometalates (TMSPs). Furthermore, the ability of lacunary polyoxoanions to incorporate magnetic TM clusters between nonmagnetic POM matrixes makes them especially valuable for the quantification of magnetic interactions.To date, the progress in TMSP chemistry chiefly focus on synthesis and characterization of new POMs possessing unique structures and properties, but the rational design and synthesis of these materials remains a longstanding challenge. Past advances have largely depended on the chance discovery of new materials.

The current trend is towards "rational design" based on the accumulated knowledge of crystal chemistry, thermodynamics and reactivity, as well as the relationship between structures and properties. Since 1970s, the functionalization of lacunary Keggin polyoxoanions by TM cations has been heavily exploited, directly resulting in the appearance of the largest inorganic sandwich-type subfamily, in which the typical structural types mainly include: mono-nuclear TM sandwiched species $[M(\alpha\text{-}PW_{11}O_{39})_2]^{10-}$ and $[M(\alpha_2\text{-}P_2W_{17}O_{61})_2]^{16-}$ ($M=Zr^{IV}/Hf^{IV}$);[4] di-nuclear: $[(\alpha\text{-}AsW_9O_{33})_2WO(H_2O)M_2(H_2O)_2]^{10-}$ ($M=Zn^{II}/Mn^{II}/Co^{II}$),[5a] $[Cs^2K(H_2O)_7Pd_2WO(H_2O)(A\text{-}\alpha\text{-}SiW_9O_{34})_2]^{9-}$,[5b] and $[(NaOH_2)_2M_2(P_2W_{15}O_{56})_2]^{18-}$ ($M=Co^{II}/Fe^{II}$)[5c,d] (Figure 1a); trinuclear: $[(\alpha\text{-}XW_9O_{33})_2M_3(H_2O)_3]^{n-}$ ($M=Cu^{II}/Zn^{II}$; $X=As^{III}/Sb^{III}/Se^{IV}/Te^{IV}$),[5a,e] $[Zr_3(OH)_3(A\text{-}\beta\text{-}SiW_9O_{34})_2]^{11-}$,[6] and $[(NaOH_2)Co_3(H_2O)(P_2W_{15}O_{56})_2]^{17-}$[5c] (Figure 1b,c); tetranuclear: $[(Mn(H_2O)_3)_2(Mn(H_2O)_2)_2(TeW_9O_{33})_2]^{8-}$,[5e] $[M_4(H_2O)_2(XW_9O_{34})_2]^{n-}$ ($M=Mn^{II}/Co^{II}/Zn^{II}/Co^{II}/Ni^{II}$; $X=P^V/Si^{IV}/Ge^{IV}$),[2a,7a–d] $[Zr_4O_2(OH)_2(H_2O)_4(\beta\text{-}SiW_{10}O_{37})_2]^{10-}$,[7e] $[M_4(H_2O)_2(P_2W_{15}O_{56})_2]^{n-}$ ($M=Mn^{II}/Fe^{III}/Co^{II}/Ni^{II}/Cu^{II}/Zn^{II}/Cd^{II}$),[2b,3g,8] and $[Zr_4(\mu_3\text{-}O)_2(\mu_2\text{-}OH)_2(H_2O)_4(P_2W_{16}O_{59})_2]^{14-}$[8k] (Figure 1d,e); pentanuclear: $[Cu_5(OH)_4(H_2O)_2(\alpha\text{-}A\text{-}SiW_9O_{33})_2]^{10-}$,[9a] and $[Co_3W(H_2O)_2(CoW_9O_{34})_2]^{12-}$[9b–c] (Figure 1f,g); hexanuclear: $[M_6Cl_6(XW_9O_{33})_2]^{12-}$ ($M=Cu^{II}/Mn^{II}$; $X=As^{III}/Sb^{III}$),[10a] $[\{Ni_6(H_2O)_4(\mu_2\text{-}H_2O)_4(\mu_3\text{-}OH)_2\}(SiW_9O_{34})_2]^{10-}$,[10b] $[Ni_4(H_2O)_2(\alpha\text{-}NiW_9O_{34})_2]^{16-}$,[10c] and $[Fe_6(OH)_3(A\text{-}\alpha\text{-}GeW_9O_{34}(OH)_3)_2]^{11-}$,[10d] (Figure 1h–k); heptanuclear: $[Ni_7(OH)_4(H_2O)(CO_3)_2(HCO_3)(A\text{-}\alpha\text{-}SiW_9O_{34})(\beta\text{-}SiW_{10}O_{37})]^{15-}$,[10b] and $[Co_7(H_2O)_2(OH)_2P_2W_{25}O_{94}]^{16-}$[11] (Figure 1o,p); as well as an octa-Co $[(A\text{-}\alpha\text{-}SiW_9O_{34})_2Co_8(OH)_6(H_2O)_2(CO_3)_3]^{16-}$[2j] (Figure 1q). Recently, four sandwich-type POT dimers $[\{(B\text{-}\beta\text{-}SiW_9O_{33}(OH))(\beta\text{-}SiW_8O_{29}(OH)_2)Co_3(H_2O)\}_2Co(H_2O)_2]^{20-}$,[2j] $[\{Co_3(B\text{-}\beta\text{-}SiW_9O_{33}(OH))(\beta\text{-}SiW_8O_{29}(OH)_2)\}_2]^{22-}$,[12a] $[Cu_{14}(OH)_4(H_2O)_{16}(SiW_8O_{31})_4]^{16-}$,[12b] $[Cu_{10}(H_2O)_2(N_3)_4(GeW_9O_{34})_2(GeW_8O_{31})_2]^{24-}$,[12b] and doubly sandwich-type POTs $[Ni_6As_3W_{24}O_{94}(H_2O)_2]^{17-}$,[13a] $[Ni_4Mn_2P_3W_{24}O_{94}(H_2O)_2]^{17-}$,[13a] and $[((MOH_2)M_2PW_9O_{34})_2(PW_6O_{26})]^{17-}$ ($M=Mn^{II}/Co^{II}$)[13b] have been depicted by Kortz and Hill, respectively. In addition, a few inorganic–organic (2–6)-TM-sandwiched POM derivatives have been reported.[14] For instance, Hill et al demonstrated the tri-Zr^{IV}-sandwiched POTs $\{[\alpha\text{-}P_2W_{15}O_{55}(H_2O)]Zr_3(\mu_3\text{-}O)(H_2O)(L/D\text{-}tartH)[\alpha\text{-}P_2W_{16}O_{59}]\}^{15-}$ with chirality transfer through zirconium coordination centers to inorganic clusters.[14a] In general, the majority of aforementioned sandwich-type TMSPs were made by conventional aqueous solution methods.

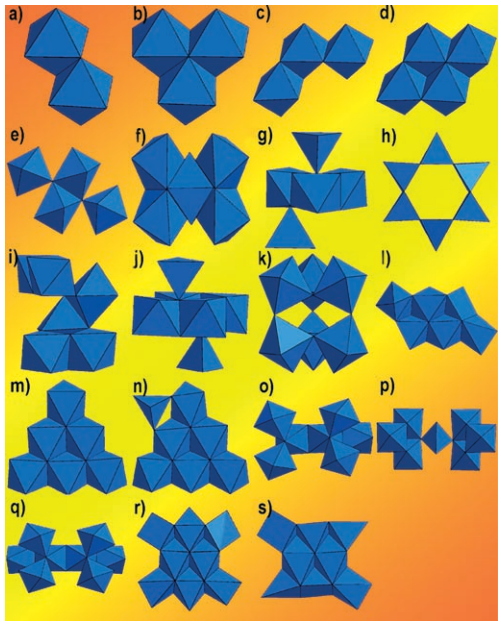

Figure 1. Polyhedral illustrations of the connection fashion of some representative transition-metal clusters previously reported (a–q) and herein investigated (r–s).

However, the combination of lacunary POM precursors and hydrothermal conditions to synthesize novel POMs remains less explored.[14b–f,15] On one hand, hydrothermal technique has been proved to be a useful method in making inorganic–organic hybrid materials in POM field. Hydrothermal conditions are able to make the reaction shift from the thermodynamic to the kinetic so that the equilibrium phases are replaced by structurally more complicated metastable phases.[16a–c] Under such nonequilibrium crystallization conditions, before lacunary POM precursors are transformed to saturated POM species, metastable kinetic POM phases rather than thermodynamic phases are most likely to be captured,[16a,d] thus we can obtain novel phases, which are not made by the conventional aqueous solution methods. On the other hand, a multitude of lacunary POM precursors provides us accessible starting materials. Thus, recently, we developed an effective method of using the lacunary sites of $[\alpha\text{-}XW_9O_{34}]^{9/10-}$ ($X=P^V/Ge^{IV}/Si^{IV}$) fragments as structure-directing agents to induce large TM oligomers and multiden-

tate N-ligands as structure-stabilizing agents to capture and stabilize the in situ generated TM oligomers or aggregates to construct novel POTs under hydrothermal conditions.[15a,b] In this manner, we have obtained a series of novel POTs $[[Ni(L)_2]_m[\{Ni_6(\mu_3\text{-}OH)_3(L)_{3-n}(H_2O)_{6+2n}\}(B\text{-}\alpha\text{-}XW_9O_{34})]\cdot y H_2O$ (L = organoamines, X = P^V/Si^{IV}), $[Cu_6(\mu_3\text{-}OH)_3(en)_3(H_2O)_3(B\text{-}\alpha\text{-}PW_9O_{34})]\cdot 7H_2O$ (Figure 1m), and $[\{Ni_7(\mu_3\text{-}OH)_3O_2(dap)_3(H_2O)_6\}(B\text{-}\alpha\text{-}PW_9O_{34})][\{Ni_6(\mu_3\text{-}OH)_3(dap)_3(H_2O)_6\}(B\text{-}\alpha\text{-}PW_9O_{34})][Ni(dap)_2(H_2O)_2]\cdot 4.5H_2O$ (Figure 1n) based on a single trivacant Keggin fragment capped by a $\{Ni_6\}/\{Cu_6\}/\{Ni_7\}$ unit.[15a,b] In the enlightenment of these findings, we think that if two trivacant $[\alpha\text{-}XW_9O_{34}]^{9/10-}$ fragments simultaneously interact with an in situ formed TM oligomer, novel sandwiched TMSPs will be formed under appropriate conditions. In an effort to realize this target, eventually, a family of inorganic–organic tetra-TM sandwiched POTs with discrete and extended structures have been isolated in our lab (Figure 1d).[14b–d] For example, we have already obtained three rare 2D tetra-TM sandwiched POTs built by sandwich-type building blocks of $[Ni_4(Hdap)_2(B\text{-}\alpha\text{-}HXW_9O_{34})_2]$ (X = $Si^{IV}/Ge^{IV}/P^V$).[14c] Whereas, a novel hexa-Cu sandwiched POT $[Cu(enMe)_2]_2\{[Cu(enMe)_2(H_2O)]_2[Cu_6(enMe)_2(B\text{-}\alpha\text{-}SiW_9O_{34})_2]\}\cdot 4H_2O$ was also isolated (Figure 1l).[14e] As an extension of our work, the reaction of $CuCl_2\cdot 2H_2O$ with trivacant Keggin precursors of $K_8Na_2[A\text{-}\alpha\text{-}GeW_9O_{34}]\cdot 25H_2O$ or $K_{10}[A\text{-}\alpha\text{-}SiW_9O_{34}]\cdot 25H_2O$ in the presence of aliphatic amines or rigid aromatic amines led to five novel inorganic–organic hybrids of octa-Cu sandwiched POTs (Figure 1r): $H_4[Cu^{II}_8(dap)_4(H_2O)_2(B\text{-}\alpha\text{-}GeW_9O_{34})_2]\cdot 13H_2O$(**1**), $(H_2en)_2[Cu^{II}_8(en)_4(H_2O)_2(B\text{-}\alpha\text{-}GeW_9O_{34})_2]\cdot 5H_2O$ (**2**), $(H_2en)_2[Cu^{II}_8(en)_4(H_2O)_2(B\text{-}\alpha\text{-}SiW_9O_{34})_2]\cdot 8H_2O$ (**3**), $[Cu^{II}(H_2O)_2]H_2[Cu^{II}_8(en)_4(H_2O)_2(B\text{-}\alpha\text{-}SiW_9O_{34})_2]$ (**4**), and $[Cu^{II}_2(H_2O)_2(2,2'\text{-}bpy)_2]\{[Cu^{II}(bdyl)]_2[Cu^{II}_8(2,2'\text{-}bpy)_4(H_2O)_2(B\text{-}\alpha\text{-}GeW_9O_{34})_2]\}\cdot 4H_2O$(**5**), besides two octa-Cu sandwiched POTs $[Cu(dap)(H_2O)_3]_2[\{Cu_8(dap)_4(H_2O)_2\}(B\text{-}\alpha\text{-}SiW_9O_{34})_2]\cdot 6H_2O$ (**7**)[15b] and $[Cu^{II}(H_2O)_2]H_2[Cu^{II}_8(dap)_4(H_2O)_2(B\text{-}\alpha\text{-}GeW_9O_{34})_2]$ (**8**)[15c] reported by us recently. Alternately, a mixture of $CuCl_2\cdot 2H_2O$, GeO_2, $Na_2WO_4\cdot 2H_2O$, $H_2SiW_{12}O_{40}\cdot 2H_2O$, 2,2′-bpy, and 4,4′-bpy afforded another mixed-valent octa-Cu sandwiched POT $[Cu^I(2,2'\text{-}bpy)(4,4'\text{-}bpy)]_2\{[Cu^I_2(2,2'\text{-}bpy)_2(4,4'\text{-}bpy)]_2[Cu^I_2Cu^{II}_6(2,2'\text{-}bpy)_2(4,4'\text{-}bpy)_2(B\text{-}\alpha\text{-}GeW_9O_{34})_2]\}\cdot 2H_2O$ (**6**) (Figure 1s). **1, 2**, and **3** are discrete dimers constructed from two trivacant Keggin $[B\text{-}\alpha\text{-}XW_9O_{34}]^{10-}$ (X = Ge^{IV}/Si^{IV}) fragments incorporating an octa-Cu cluster whereas **4** displays 3D (3,6)-connected nets with $(4\cdot 6^2)(4^2\cdot 6^4\cdot 8^7\cdot 10^2)$ topology based on octa-Cu sandwiched trivacant Keggin POMs as building blocks, which is isostructural to **8**.[15c] **5** is a novel 2D layer based on octa-Cu sandwiched POM clusters and $[Cu^{II}_2(bdyl)]$ units. Interestingly, the rollover metalation[17] of 2,2′-bpy is firstly observed in the system containing copper complex under hydrothermal conditions. **6** is a discrete mixed-valent octa-Cu sandwiched dimer supported by two symmetrical di-Cu^I complexes $[Cu^I_2(2,2'\text{-}bpy)_2(4,4'\text{-}bpy)]^{2+}$ through 4,4′-bpy bridges except for two free mono-Cu complexes $[Cu^I(2,2'\text{-}bpy)(4,4'\text{-}bpy)]^+$. To the best of our knowledge, **1**–**6** represent a novel and rare family of POTs incorporating octa-nuclear TM clusters in POM chemistry. The successful syntheses of these POTs not only further testify that the combination of lacunary POM precursors and hydrothermal conditions is an effective strategy in preparing novel hybrid inorganic–organic TMSPs, but also enrich the structural diversity of sandwich-type TMSPs.

Results and Discussion

Synthesis and IR spectra: Many inorganic TMSPs can be easily obtained based on mono-, di-, tri-, or even multivacant POM precursors by virtue of conventional aqueous solution methods under the standard pressure, especially for Keggin- and Dawson-type POTs. However, this method is not suitable to prepare hybrid inorganic–organic POTs containing octa-Cu clusters in the presence of aliphatic amines such as 1,2-diaminopropane (dap) and ethylenediamine (en) or rigid aromatic amines such as 2,2′-bipyridine (2,2′-bpy) and 4,4′-bpy. Therefore, we chose the hydrothermal method to explore this subject. Because the solubilities of different phases are increased, a variety of organic and inorganic components can be introduced. As we know, the rational design of an experiment implies two steps: the first is to identify the structural type and probable chemical compositions that would give rise to the desired properties; the next step is to find an appropriate method to make the materials.[16a] Although we are far from the ultimate dream of "tailor-making" desired products with specified structures and properties, the rational design has been possible to a limited extent within selected families of compounds. In our case, it is possible to predict the existence of new phases within the same structural types by analogy to already known phases.

At the beginning, the reaction of the trivacant Keggin polyoxoanion $[A\text{-}\alpha\text{-}SiW_9O_{34}]^{10-}$ ($A\text{-}\alpha\text{-}SiW_9$) with the Cu^{II} ion in the presence of dap resulted in the first hybrid inorganic–organic octa-Cu sandwiched POT **7**[15b] (Table 1). With the further exploitation of our experiments, we also isolated another two silicotungstates, **3** and **4**. The structure of **3** is very similar to that of **7**,[15b] however, **4**, unlike **3**, is a novel 3D structure with a $(4\cdot 6^2)(4^2\cdot 6^4\cdot 8^7\cdot 10^2)$ topological net. Considering the structural similarity between $[A\text{-}\alpha\text{-}GeW_9O_{34}]^{10-}$ ($A\text{-}\alpha\text{-}GeW_9$) and $A\text{-}\alpha\text{-}SiW_9$, if $A\text{-}\alpha\text{-}GeW_9$ was employed, three hybrid inorganic–organic germanotungstates **1**, **2** and **8**[15c] were consecutively separated. **2** and **8**[15c] are isostructural to **3** and **4**, respectively. Unfortunately, if $[A\text{-}\alpha\text{-}PW_9O_{34}]^{10-}$ ($A\text{-}\alpha\text{-}PW_9$) was introduced, a completely distinct POT $[Cu_6(en)_3(H_2O)_3(OH)_3][B\text{-}\alpha\text{-}PW_9O_{34}]\cdot 7H_2O$ (**9**) was afforded. POT **9** was recently reported by us,[15b] with a 3D 4^96^6 "Archimedean-type" net built by hexa-Cu incorporated trivacant Keggin-type phosphotungstate units. Hitherto, the octa-Cu sandwiched phosphotungstate have not been synthesized in our lab so far, we think that the key factor may be intimately related to the nature of $A\text{-}\alpha\text{-}PW_9$.

These intriguing results ignited and spurred on our intensive interest. Can the replacement of dap/en with 2,2′-bipy

Table 1. Summary of synthetic conditions and related phases in the preparations of **1–5**.

Reactant	Molar ratio of reactants	*T* [°C]	Phase
A-α-SiW_9[a]/$CuCl_2$·2H_2O/dap/H_2O	0.097/0.75/0.589/278	100	**7**[15b]
A-α-SiW_9/$CuCl_2$·2H_2O/en/H_2O	0.097/0.10/0.74/278	100	**3**
A-α-SiW_9/$CuCl_2$·2H_2O/en/H_2O	0.08/1.25/0.74/278	100	**4**
A-α-GeW_9[b]/$CuCl_2$·2H_2O/dap/H_2O	0.08/0.75/0.589/278	100	**8**[15b]
A-α-GeW_9/$CuCl_2$·2H_2O/en/H_2O	0.08/1.25/0.74/278	100	**2**
A-α-GeW9/$CuCl_2$·2H_2O/2,2′-bpy/4,4′-bpy/H_2O	0.12/0.5/0.25/0.50/444	150	**5**
A-α-GeW9/$CuCl_2$·2H_2O/2,2′-bpy/4,4′-bpy	0.08/0.5/0.25/0.25/444	150	**10**[18a]
GeO_2/Na_2WO_4·2H_2O/$H_2SiW_{12}O_{40}$·2H_2O[c]/$CuCl_2$·2H_2O/2,2′-bpy/4,4’-bpy/H_2O	0.15/0.6/0.6/0.15/0.13/0.065/278	170	**5**
GeO_2/Na_2WO_4·2H_2O/$H_2SiW_{12}O_{40}$·2H_2O[c]/$CuCl_2$·2H_2O/2,2′-bpy/4,4’-bpy/H_2O	0.15/0.6/0.15/0.13/0.06/5/278	170	**6**
GeO_2/Na_2WO_4·2H_2O/$H_2SiW_{12}O_{40}$·2H_2O[c]/$CuCl_2$·2H_2O/2,2′-bpy/4,4’-bpy/H_2O	0.15/0.6/0.15/0.13/0.06/5/278	170	**10**[18a]
GeO_2/Na_2WO_4·2H_2O/$H_2SiW_{12}O_{40}$·2H_2O[c]/$CuCl_2$·2H_2O/2,2′-bpy/4,4’-bpy/H_2O	0.15/0.6/0.15/0.154/278	170	**11**[18a]
A-α-PW_9[d]/$CuCl_2$·2H_2O/en/H_2O	0.094/1.0/0.74/278	80	**9**[15b]

[a] A-α-SiW_9: K_{10}[A-α-SiW_9O_{34}]·25H_2O. [b] A-α-GeW_9: K_8Na_2[A-α-GeW_9O_{34}]·25H_2O[10d] [c] $H_2SiW_{12}O_{40}$·2H_2O is the commercial material. [d] A-α-PW_9: Na_9[A-α-PW_9O_{34}] ·7H_2O[3e]

A comparison of **1–4** with **5–6** shows that they all contain octa-Cu cluster units, but the formation pH values are different. For **1–4**, the initial pH values vary between 3.5–4.5, whereas for **5–6**, the starting pH values range between 9.0–10.5. Under the pH values similar to **1–4**, **5–6** can not be made. In contrast, under the pH values similar to **5–6**, **1–4** can not be obtained. As a result, we conjecture that the formation of **1–6** may be related to the basicity of ligands.

It is necessary that the transformation between isomers occurred in the formation of **1–5**. Compounds **1, 2**, and **5** inevitably experienced the isomerization of A-α-GeW_9→B-α-GeW_9. In the formation of **3** and **4**, the isomerization of A-α-SiW_9→B-α-SiW_9 was also observed. The isomerization of A-α-GeW_9→B-α-GeW_9 was previously observed in conventional aqueous solution[5b] and under hydrothermal conditions,[15c] respectively. Furthermore, the isomerization behaviors between different silicotungstate polyoxoanions in aqueous solution were systematically studied by Tézé et al and well understood.[3c] This isomerization of A-α-XW_9→B-α-XW_9 ($X=Ge^{IV}/Si^{IV}$) may be closely related to the reaction conditions and the stability of the resulting products. On one hand, if the reaction is carried out under heating condition, it is favorable for this isomerization of A-α-XW_9→B-α-XW_9,[15b,19] which is in good agreement with the driving force of isomerization controlled by the thermodynamic factors.[19a] On the other hand, the A-α-XW_9 unit has six exposed surface oxygen atoms in the vacant site, whereas the B-α-XW_9 unit has seven exposed surface oxygen atoms in the vacant site, therefore, the B-α-XW_9 unit can work as a heptadentate ligand to coordinate to the in situ generated TM clusters and further enhance the stability of the resulting compounds.[15b]

The IR spectra of **1–6** have been recorded between 4000 and 400 cm^{-1} and display four characteristic vibration patterns derived from the Keggin framework in $\tilde{\nu}=600$–1000 cm^{-1}, namely, $\nu(W{-}O_t)$, $\nu(X{-}O_a)$ ($X=Ge^{IV}/Si^{IV}$), $\nu(W{-}O_b)$, and $\nu(W{-}O_c)$. In the IR spectra of **1–4**, the stretching bands of -OH, -NH_2, and -CH_2 groups are observed at $\tilde{\nu}=$ 3420–3450, 3100–3350, and 2950–3000 cm^{-1}, respectively and the bending vibration bands of -NH_2 and -CH_2 groups also appear at $\tilde{\nu}=1570$–1640 and 1450–1470 cm^{-1}, respectively. The occurrence of these resonance signals confirms the presence of amino groups in **1–4**. In the IR spectra of **5**, four vibration peaks at $\tilde{\nu}=1473$, 1447, 1318, and 1252 cm^{-1} are indicative of 2,2′-bpy and are in good agreement with the reported characteristic vibration peaks of 2,2′-bpy.[18b] In the IR spectrum of **6**, in addition to the four characteristic vi-

or 4,4′-bpy form octa-Cu sandwiched POTs? After many experiments, we finally made a 2,2′-bpy-containing octa-Cu sandwiched germanotungstate **5**. Notably, 4,4′-bpy is very necessary in making **5**, although it is not found in the structure of **5**. The role of 4,4′-bpy is not well understood to date. Unfortunately, similar silicotungstates and phosphotungstates have still not been harvested. Further investigations are in progress. During the course of our exploration, we also obtained another novel copper-complex-substituted POT dimer {[Cu^{II}_5(2,2′-bpy)$_5$(H_2O)][B-α-GeW_9O_{34}]}$_2$·7H_2O (**10**),[18a] which contains two hybrid trivacant {[Cu^{II}(2,2′-bpy)]$_4$[B-α-GeW_9O_{34}]}$^{2-}$ units linked by two five-coordinate [Cu^{II}(2,2′-bpy)(H_2O)]$^{2+}$ bridges. Although a tetravacant Keggin POT dimer Na_2[{Cu_8(2,2′-bpy)$_8$}(PW_8O_{31})$_2$]·7H_2O, which is very similar to **10**, was reported by Lisnard et al by virtue of a mixture of Na_2WO_4·2H_2O, $CuCl_2$·2H_2O, 2,2′-bpy, H_3PO_4, and H_2O under 160 °C hydrothermal conditions,[18b] to date we still have not obtained similar silicotungstates and phosphotungstates by the reaction of α-XW_9 ($X=Si^{IV}$/P^V) fragments with Cu^{II} ions. To extend our work, we reacted $CuCl_2$·2H_2O with a mixture of GeO_2, Na_2WO_4·2H_2O, $H_2SiW_{12}O_{40}$·2H_2O in the presence of 2,2′-bpy and 4,4′-bpy, **5** and an unprecedented mixed-valent octa-Cu sandwiched germanotungstate **6** were successfully obtained. In the absence of $H_2SiW_{12}O_{40}$·2H_2O, under similar conditions to those of **5** and **6**, we harvested two copper-complex-substituted tungstogermanates **10** and [Cu^{II}_5(2,2′-bpy)$_6$(H_2O)][B-β-GeW_8O_{31}]·9H_2O (**11**),[18a] which are distinct from **5** and **6**. Compound **11** is a tetravacant β-Keggin [β-B-GeW_8O_{31}]$^{10-}$ polyoxoanion supported by five Cu^{II}-2,2′-bpy coordination cations. Experimental results proved that when $H_2SiW_{12}O_{40}$·2H_2O was removed from the reaction system, **5** and **6** could not be isolated. The role of $H_2SiW_{12}O_{40}$·2H_2O is not well understood. Until now, **6** could not be obtained by the reaction of A-α-GeW_9 with Cu^{II} ions in the presence of 2,2′-bpy and 4,4′-bpy.

bration peaks of 2,2′-bpy, two vibration peaks at $\tilde{\nu}=1410$ and 1220 cm^{-1} denote the presence of 4,4′-bpy.[18b]

Structures of $H_4[Cu^{II}_8(dap)_4(H_2O)_2(B\text{-}\alpha\text{-}GeW_9O_{34})_2]\cdot 13H_2O$ (1) $(H_2en)_2[Cu^{II}_8(en)_4(H_2O)_2(B\text{-}\alpha\text{-}GeW_9O_{34})_2]\cdot 5H_2O$ (2) and $(H_2en)_2[Cu^{II}_8(en)_4(H_2O)_2(B\text{-}\alpha\text{-}SiW_9O_{34})_2]\cdot 8H_2O$ (3): The structure of **1** crystallizes in the monoclinic space group $P2_1/c$, whereas both **2** and **3** are isostructural and crystallize in the monoclinic space group $P2_1/n$ (Table 2). The molecular structure consists of a dimeric polyoxoanion $[Cu^{II}_8(dap)_4(H_2O)_2(B\text{-}\alpha\text{-}GeW_9O_{34})_2]^{4-}$ (**1a**) for **1** (Figure 2a) and $[Cu^{II}_8(en)_4(H_2O)_2(B\text{-}\alpha\text{-}XW_9O_{34})_2]^{4-}$ ($X=Ge^{IV}/Si^{IV}$) for **2** and **3** (Figure S1a in the Supporting Information), which are all built by two B-α-XW_9 fragments and an octa-Cu cluster. Therefore, only **1** is described in detail. The dimeric **1a** can be considered as a fusion of two $[Cu^{II}_4(dap)_2(H_2O)(B\text{-}\alpha\text{-}GeW_9O_{34})]^{2-}$ subunits symmetrically related by an inversion center (0, ½, 0), in which two staggered B-α-GeW_9 fragments are linked by eight Cu^{II} ions through eight μ_3-O and four μ_4-O atoms from lacunae of two B-α-GeW_9 fragments and two μ_4-O atoms from two GeO_4 groups, resulting in a novel sandwich-type structure (Figure 2a).

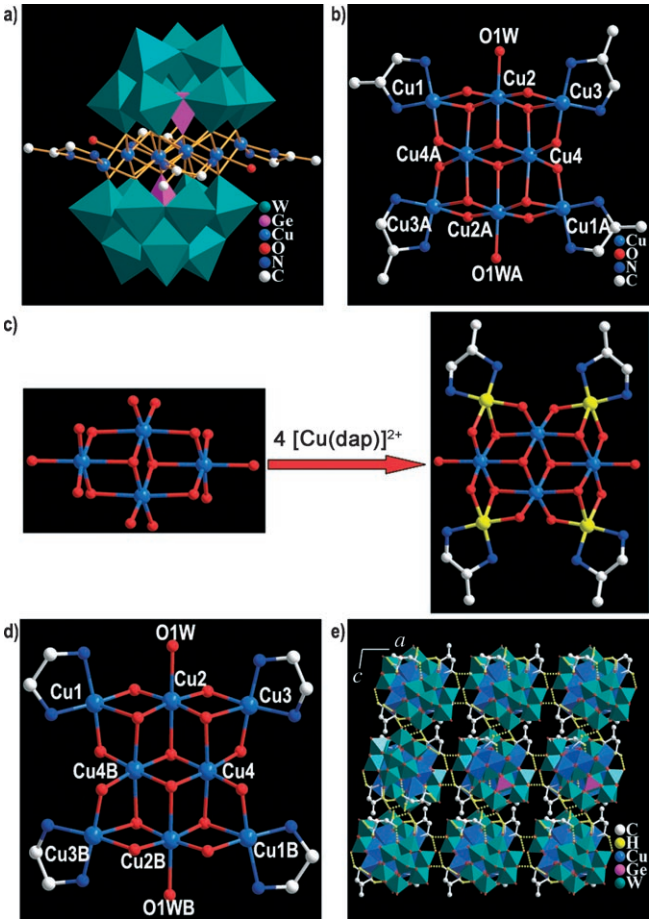

Figure 2. a) Ball-and-stick/polyhedral representation of **1a**. b) The connection motif of the $\{[Cu(dap)]_4Cu_4O_{14}(H_2O)_2\}$ cluster in **1a**. Atoms with "A" in their labels are symmetrically generated (A: $-x$, $1-y$, $-z$). c) Relationship between the tetra-Cu cluster $\{Cu^{II}_4O_{14}(H_2O)_2\}$ in the $[Cu^{II}_4(H_2O)_2(B\text{-}\alpha\text{-}GeW_9O_{34})_2]^{12-}$ polyoxoanion and the octa-Cu cluster $\{[Cu^{II}(dap)]_4Cu^{II}_4O_{14}(H_2O)_2\}$ in **1**. d) The connection motif of the $\{[Cu(en)]_4Cu_4O_{14}(H_2O)_2\}$ cluster in **3**. Atoms with "B" in their labels are symmetrically generated (B: $1-x$, $-y$, $-z$). e) The packing arrangement of **1** along the *b* axis, and the yellow dashed bonds represent the hydrogen-bonding interactions.

It is of special interest to investigate the structure of the octa-Cu^{II} $\{[Cu(dap)]_4Cu_4O_{14}(H_2O)_2\}$ cluster in **1a** (Figure 2b). Eight Cu^{II} cations are almost coplanar in the motif of 3:2:3, leading to three types of the coordination environments: the first type (two Cu1, two Cu3) resides in a five-coordinate square pyramid, in which the basal plane is defined by two N atoms from a bidentate dap ligand [Cu–N: 1.958(17)–2.01(2) Å] and two μ_3-O atoms from two B-α-GeW_9 fragments [Cu-μ_3-O: 1.978(13)–2.011(15) Å] and one μ_4-O atom from a B-α-GeW_9 fragment occupies the apical position [Cu–O: 2.394(15)–2.442(14) Å]; the second (two Cu2) is a six-coordinate octahedral geometry with two μ_3-O and two μ_4-O atoms from two B-α-GeW_9 fragments building the equatorial plane [Cu-μ_3-O: 1.984(14)–1.988(14) Å and Cu-μ_4-O: 1.993(13)–2.022(14) Å], and one μ_4-O atom from a GeO_4 group and one water O atom standing on the axial positions [Cu-μ_4-O: 2.336(13) Å and Cu–O_W: 2.278(18) Å]; the third (two Cu4) has two μ_3-O and two μ_4-O atoms from two B-α-GeW_9 fragments in the square planar coordination [Cu-μ_3-O: 1.947(14)–1.978(13) Å and Cu-μ_4-O: 1.981(12)–1.985(12) Å], and its coordination sphere is completed by two μ_4-O atoms from two B-α-GeW_9 fragments [Cu-μ_4-O: 2.413(14)–2.415(14) Å]. To our knowledge, such a coplanar octa-Cu cluster is novel, not only in coordination chemistry, but also in POM chemistry. The octa-Cu cluster is formed by four interior $Cu^{II}O_6$ octahedra and four exterior $Cu^{II}O_3N_2$ square pyramids in the edge-sharing fashion (Figure 1r), in which four exterior $Cu^{II}O_3N_2$ groups have two coordination orientations: the pyramidal vertices of two $Cu^{II}O_3N_2$ groups point to one side of the plane defined by eight Cu^{II} ions, whereas the pyramidal vertices of the other two $Cu^{II}O_3N_2$ groups point to the other side of the plane. Additionally, four interior edge-sharing CuO_6 groups form a centrosymmetric rhomboid-like cluster $\{Cu_4O_{14}(H_2O)_2\}$, which was observed in a tetra-Cu^{II} sandwiched $[Cu_4(H_2O)_2(B\text{-}\alpha\text{-}GeW_9O_{34})_2]^{12-}$,[7d] as a consequence, **1a** can be considered as a novel derivative of $[Cu_4(H_2O)_2(B\text{-}\alpha\text{-}GeW_9O_{34})_2]^{12-}$. The octa-Cu cluster $\{[Cu(dap)]_4Cu_4O_{14}(H_2O)_2\}$ in **1a** can also be considered that four exogenous five-coordinate $[Cu(dap)]^{2+}$ cations graft to four corners of the rhombic cluster $\{Cu_4O_{14}(H_2O)_2\}$ in $[Cu_4(H_2O)_2(B\text{-}\alpha\text{-}GeW_9O_{34})_2]^{12-}$ through twelve oxygen atoms from the lacunae of two B-α-GeW_9 fragments (Figure 2c). Furthermore, the $\{[Cu(en)]_4Cu_4O_{14}(H_2O)_2\}$ clusters in **2** and **3** are very similar to that in **1** (Figure 2d). Owing to the coexistence of octahedral and square pyramidal geometries of Cu^{II} ions, the Jahn–Teller effect of octahedra, pseudo-Jahn–Teller effect of square pyramids and different linkage modes possibly lead to different isomers or configurations. In **1**, all the Cu^{II} ions exhibit the axial elongation, whereas in **8**,[15c] Cu1, Cu2, and Cu3 ions exhibit the axial elongation and Cu4 ion shows the axial compression. Moreover, one copper-substi-

Table 2. X-ray crystallographic data for **1–6.**

	1	**2**[c]	**3**
empirical formula	$C_{12}H_{74}N_8O_{83}Cu_8Ge_2W_{18}$	$C_{12}H_{66}N_{12}O_{75}Cu_8Ge_2W_{18}$	$C_{12}H_{72}N_{12}O_{78}Cu_8Si_2W_{18}$
formula weight	5621.59	5541.57	5506.62
crystal system	monoclinic	monoclinic	monoclinic
space group	$P2_1/c$	$P2_1/n$	$P2_1/n$
a [Å]	13.2438(1)	13.417(3)	13.2929(17)
b [Å]	16.5562(2)	21.315(8)	21.195(4)
c [Å]	23.6087(1)	15.780(4)	15.591(2)
α [°]	90	90	90
β [°]	98.696(1)	91.009(10)	91.674(7)
γ [°]	90	90	90
V [Å^3]	5117.10(8)	4512(2)	4390.6(11)
Z	2	2	2
ρ_c [g cm^{-3}]	3.649	4.079	4.165
absorption coefficient, mm^{-1}	22.436	25.435	25.500
T [K]	293(2)	293(2)	293(2)
limiting indices	$-13\le h\le 16$	$-15\le h\le 15$	$-15\le h\le 15$
	$-15\le k\le 20$	$-25\le k\le 20$	$-25\le k\le 17$
	$-28\le l\le 26$	$-18\le l\le 18$	$-18\le l\le 18$
no. of reflections collected	27426	26920	25864
no. of independent reflections	9630	7913	7420
data/restrains/parameters	9630/6/572	7913/12/471	7420/38/519
goodness-of-fit on F^2	1.103	1.096	1.097
final R indices [$I>2\sigma(I)$]			
R_1	0.0618[a]	0.1793	0.0797
wR_2	0.1110[b]	0.4180	0.1813
R indices (all data)			
R_1	0.1177	0.1970	0.0875
wR_2	0.1327	0.4271	0.1855
	4	**5**	**6**
empirical formula	$C_8H_{42}Cu_9N_8O_{72}Si_2W_{18}$	$C_{80}H_{76}Cu_{12}Ge_2N_{16}O_{76}W_{18}$	$C_{140}H_{116}Cu_{14}Ge_2N_{28}O_{70}W_{18}$
formula weight	5339.84	6694.53	7654.65
crystal system	tetragonal	monoclinic	triclinic
space group	$P4_2/ncm$	$C2m$	$P\bar{1}$
a [Å]	21.3874(13)	21.308(8)	15.374(2)
b [Å]	21.3874(13)	22.250(7)	15.958(2)
c [Å]	18.634(2)	17.756(6)	20.163(4)
α [°]	90	90	96.988(12)
β [°]	90	121.366(3)	108.544(7)
γ [°]	90	90	108.919(8)
V [Å^3]	8523.4(12)	7188(4)	4295.0(12)
Z	4	2	1
ρ_c [g cm^{-3}]	4.161	3.093	2.959
absorption coefficient, mm^{-1}	26.499	16.569	14.123
T [K]	293(2)	293(2)	293(2)
limiting indices	$-25\le h\le 25$	$-25\le h\le 25$	$-16\le h\le 18$
	$-25\le k\le 21$	$-26\le k\le 15$	$-18\le k\le 18$
	$-22\le l\le 21$	$-21\le l\le 21$	$-23\le l\le 23$
no. of reflections collected	51668	23017	27445
no. of independent reflections	3859	6514	14887
data/restrains/parameters	3859/1/285	6514/86/523	14887/17/1027
goodness-of-fit on F^2	1.077	1.049	1.009
final R indices [$I>2\sigma(I)$]			
R_1	0.0747	0.0656	0.0512
wR_2	0.1870	0.1668	0.1332
R indices (all data)			
R_1	0.0834	0.0909	0.656
wR_2	0.1966	0.1801	0.1451

[a] $R_1=\Sigma||F_o|-|F_c||/\Sigma|F_o|$. [b] $wR_2=[\Sigma w(F_o^2-F_c^2)^2/\Sigma w(F_o^2)^2]^{1/2}$; $w=1/[\sigma^2(F_o^2)+(xP)^2+yP]$, $P=(F_o^2+2F_c^2)/3$, in which $x=0.0276$, $y=270.2291$ for **1**, $x=0.1134$, $y=3502.4368$ for **2**, $x=0.0520$, $y=859.8872$ for **3**, $x=0.1155$, $y=0.0000$ for **4**, $x=0.0851$, $y=565.6891$ for **5** and $x=0.0923$, $y=0.0000$ for **6.** [c] Although the final residuals (R_1/wR_2) are somewhat large, owing to poor crystal quality, the POM backbone and organic ligands in **2** are well behaved, and there are no unusual temperature factors in the structure.

tuted POT $K_7Na[Cu^{II}{}_4K_2(H_2O)_6(\alpha\text{-}AsW_9O_{33})_2]\cdot 5.5H_2O$ including simultaneously the axial elongation/compression of Cu^{II} ions.[20] In addition, since the adjacent Cu···Cu distances are in the range of 3.057–3.209 Å and Cu-O-Cu angles vary

in 80.6(5)–107.1 (6)° in **1**, competitive ferromagnetic and antiferromagnetic interactions are expected in such a system mediated by oxo-bridges.

It should be mentioned that the assembly of metal-involved supramolecular architectures is currently of great interest in the field of supramolecular chemistry and crystal engineering because they can provide novel topology and functional materials.[21] Moreover, Keggin-based supramolecular architectures are regarded as one of the most promising materials potentially applied in the field of chemistry, biology and material sciences.[22] From the viewpoint of supramolecular chemistry, supramolecular architectures are also present in **1**–**3** taking into account hydrogen-bonding interactions between the nitrogen atoms of amine ligands and the surface oxygen atoms of polyoxoanions and water molecules (Figure 2e, and S1b in the Supporting Information). The N-H···O distances are in the range of 2.94(3)–3.32(3) Å for **1**, 2.73(10)–3.24(10) Å for **2**, and 2.17(6)–3.29(3) Å for **3**, respectively.

Except several POTs sandwiching coplanar octa-Cu clusters reported in our previous[15b–c] and present papers, only two POTs sandwiching coplanar hexa-Cu clusters have been addressed by Yamase's group and our group in 2006 and 2007 respectively,[10a,14e] in which the coplanar hexa-Cu clusters adopt two distinct distribution motifs: in $(n\mathrm{BuNH_3})_{12}$-$[Cu^{II}_6Cl_6(B\text{-}\alpha\text{-}AsW_9O_{33})_2]\cdot 4H_2O$,[10a] the hexa-Cu cluster with D_{3d} symmetry shows an equatorial hexagonal alignment formed by the edge-sharing mode (Figure 1h), in which each Cu^{II} ion is square-pyramidally coordinated by four O atoms from two $[B\text{-}\alpha\text{-}AsW_9O_{33}]^{9-}$ fragments and an exterior Cl ion; whereas in $[Cu^{II}(enMe)_2]_2\{[Cu^{II}(enMe)_2(H_2O)]_2$-$[Cu^{II}_6(enMe)_2(B\text{-}\alpha\text{-}SiW_9O_{34})_2]\}\cdot 4H_2O$,[14e] the hexa-Cu cluster with C_i symmetry exhibits a belt-like arrangement generated by the edge-sharing mode (Figure 1l), in which there are three kinds of Cu^{II} coordination environments, two central Cu^{II} ions octahedrally coordinated by six O atoms from two B-α-SiW_9 fragments, two Cu^{II} ions square-pyramidally coordinated by five O atoms from two B-α-SiW_9 fragments, and two Cu^{II} ions square-pyramidally coordinated by three O atoms from two B-α-SiW_9 fragments and two N atoms from enMe ligands.[14e] Very recently, a new POT $[Cu_{14}(OH)_4(H_2O)_{16}(SiW_8O_{31})_4]^{16-}$ was reported by Wang et al,[12b] in which the hexa-Cu cluster sandwiched by two $[\beta\text{-}SiW_8O_{31}]^{10-}$ fragments exhibits C_2 symmetry, although six Cu^{II} ions have octahedral geometries, they are not situated on one plane: three CuO_6 octahedra are edge-sharing to form a trigonal trimer, the remaining three are also edge-sharing and generate a linear trimer, and then two trimers are further linked by two corner-sharing vertices (Figure S2 in the Supporting Information). Additionally, a *C*-shaped octa-Co-incorporated silico-tungstate with a discrete structure, $K_8Na_8[(A\text{-}\alpha\text{-}SiW_9O_{34})_2Co_8(OH)_6(H_2O)_2(CO_3)_3]\cdot 52H_2O$, was recently reported by Mialane et al,[2j] in which two $\{Co_4O_9(OH)_3(H_2O)\}$ clusters are linked edge-shared through three carbonato groups (Figure 1q). The structures **1**–**3**, and **7** represent rare, discrete, inorganic–organic octa-Cu sandwiched POTs, whereas **4** and **8** represent unique, 3D, hybrid-inorganic–organic octa-Cu sandwiched POTs with a $(4\cdot6^2)(4^2\cdot6^4\cdot8^7\cdot10^2)$ topology in POM chemistry.

Structure of $[Cu^{II}(H_2O)_2]H_2[Cu^{II}_8(en)_4(H_2O)_2(B\text{-}\alpha\text{-}SiW_9O_{34})_2]$ (4): Different from **1, 2**, and **3**, compound **4** crystallizes in the tetragonal space group $P4_2/ncm$. In **1, 2**, and **3**, a crystallographic imposed C_2 axis passes through an inversion center (0, 0.5, 0) and (0.5, 0, 0), respectively, whereas in **4** there is a crystallographically imposed C_4 axis that passes through an inversion center (0, 0.5, 0). The structural unit of **4** consists of a dimeric unit $[Cu^{II}_8(en)_4(H_2O)_2(B\text{-}\alpha\text{-}SiW_9O_{34})_2]^{4-}$ (**4a**) and one $[Cu^{II}(H_2O)_2]^{2+}$ cation (Figure 3a). The connection mode of the octa-Cu^{II} cluster $\{[Cu^{II}(en)]_4Cu^{II}_4O_{14}(H_2O)_2\}$ (Figure 3b) in **4** is similar to that in **1**, therefore, we do not discuss it here. However, it is of special interest that adjacent dimeric units **4a** are connected by $[Cu^{II}4(H_2O)_2]^{2+}$ bridges constructing a 3D framework that is isostructural to $[Cu^{II}(H_2O)_2]H_2[Cu^{II}_8(dap)_4(H_2O)_2(B\text{-}\alpha\text{-}GeW_9O_{34})_2]$ (**8**) recently reported by us.[15c]

The most striking structural feature of **4** is that each **4a** joins an adjacent six $[Cu4(H_2O)_2]^{2+}$ bridges (Figure 3a), each $[Cu4(H_2O)_2]^{2+}$ bridge links to an adjacent three **4a** units (Figure 3c), leading to a novel 3D (3,6)-connected network. The inerratic arrangements of such **4a** units and $[Cu4(H_2O)_2]^{2+}$ bridges along the 4_2 screw axis result in two types of small helical channels (A and B) with the cross-section sizes of 2.5×2.5 Å and 1.3×1.3 Å along the *c*-axis (Figure 3d). Notably, channels A and B are enclosed by two couple of interweaved dual left-/right helices, L1/R1 and L2/R2, with a pitch of 18.63 Å (Figure 3e). For L1/R1 chains, each chain is built by **4a** units through the $[Cu4(H_2O)_2]^{2+}$ bridges. The en ligands and the terminal O atoms of B-α-SiW_9 units protrude into the inner of A channels. There exist the hydrogen-bonding interactions between N atoms of en ligands and O atoms of B-α-SiW_9 units (N-H···O: 3.02(3)–3.19(2) Å). For L2/R2 chains, each chain is constructed from the $[Cu4(H_2O)_2]^{2+}$ cations through **4a** units. Different from A channels, the coordination water molecules from $[Cu4(H_2O)_2]^{2+}$ cations point to the inner of B channels. Although two 3D architectures with helical channels built by plenary Keggin units and amino acid complexes[23] and a novel 3D architecture with hexagonal channels enclosed by three inter-weaved helical chains constructed from hexa-Cu^{II} clusters and trivacant Keggin B-α-PW_9 fragments[15b] have been reported, to our knowledge, **4** and **8** represent the first 3D (3,6)-connected trivacant Keggin derivatives with helical channels based on the octa-Cu sandwiched POTs as building blocks. Topologically, the nonpenetrating 3D (3,6)-connected network can be simplified by considering that each dimer **4a** is regarded as a 6-connected node and every $[Cu4(H_2O)_2]^{2+}$ functions as 3-connected node, the resulting net is shown in Figure 3f. The 6- and 3-connected nodes are in the ratio 1:2. A topological analysis of this net was performed with OLEX.[24] The Schäfli symbol of this net is $(4\cdot6^2)(4^2\cdot6^4\cdot8^7\cdot10^2)$.

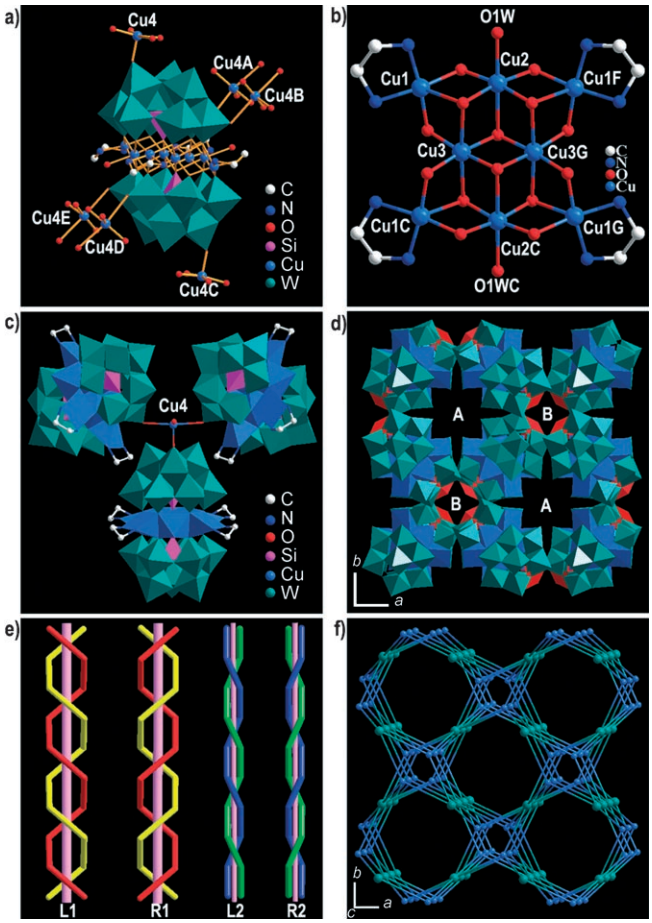

Figure 3. a) Coordination environment of the dimeric unit **4a**. b) The connection motif of the $\{[Cu^{II}(en)]_4Cu^{II}_4O_{14}(H_2O)_2\}$ cluster in **4**. Atoms with "A–G" in their labels are symmetry-generated (A: y, $0.5-x$, $-0.5+z$; B: $0.5-y$, x, $-0.5+z$; C: $-0.5+y$, $0.5+x$, $-z$; D: $-0.5+x$, $1-y$, $0.5-z$; E: $-x$, $0.5+y$, $0.5-z$; F: $0.5-y$, $0.5-x$, z; G: $-x$, $1-y$, $-z$). c) The combination of one $[Cu4(H_2O)_2]^{2+}$ ion and three **4a** units. d) The 3D framework viewed down the *c*-axis, revealing two types of A and B helical channels. The $[Cu4(H_2O)_2]^{2+}$ bridges are highlighted in red polyhedra. The carbon and hydrogen atoms are omitted for clarity. e) The dual left-/right-handed helices (L1/R1 and L2/R2) enclosing two different A and B channels, respectively. For clarity, L1/R1 helices are only shown in **4a** nodes, and $[Cu4(H_2O)_2]^{2+}$ bridges are omitted, whereas L2/R2 helices are only shown in $[Cu4(H_2O)_2]^{2+}$ nodes, and **4a** bridges are omitted. f) The 3D $(4{\cdot}6^2)$ $(4^2{\cdot}6^4{\cdot}8^7{\cdot}10^2)$ net along the c-axis. Dark green: **4a** nodes; Blue: $[Cu4(H_2O)_2]^{2+}$ nodes.

Structure of $[Cu^{II}_2(H_2O)_2(2,2'\text{-bpy})_2]\{[Cu^{II}(bdyl)]_2[Cu^{II}_8(2,2'\text{-bpy})_4(H_2O)_2(B\text{-}\alpha\text{-}GeW_9O_{34})_2]\}\cdot 4H_2O$ (5): Structure **5** crystallizes in the monoclinic space group $C2m$. Its molecular unit (Figure 4a) consists of an unprecedented POT dimer supported by four $[Cu_2(bdyl)]^{2+}$ bridges, $\{[Cu(bdyl)]_2[Cu_8(2,2'\text{-bpy})_4(H_2O)_2(B\text{-}\alpha\text{-}GeW_9O_{34})_2]\}^{4-}$ (**5a**) (Figure 4b), a dimeric cation $[Cu_2(H_2O)_2(2,2'\text{-bpy})_2]^{4+}$ and four lattice water molecules. Notably, the bdyl ligand on the supported $[Cu_2(bdyl)]^{2+}$ groups is derived from 2,2′-bpy by eliminating two protons, and adopts an unique *trans*-four-coordination mode to bond two Cu^{II} atoms, resulting in a novel $[Cu_2(bdyl)]^{2+}$ group. The linking mode of two B-α-GeW_9 and one $\{[Cu(2,2'\text{-bpy})]_4Cu_4O_{14}(H_2O)_2\}$ cluster in **5** is similar to those in

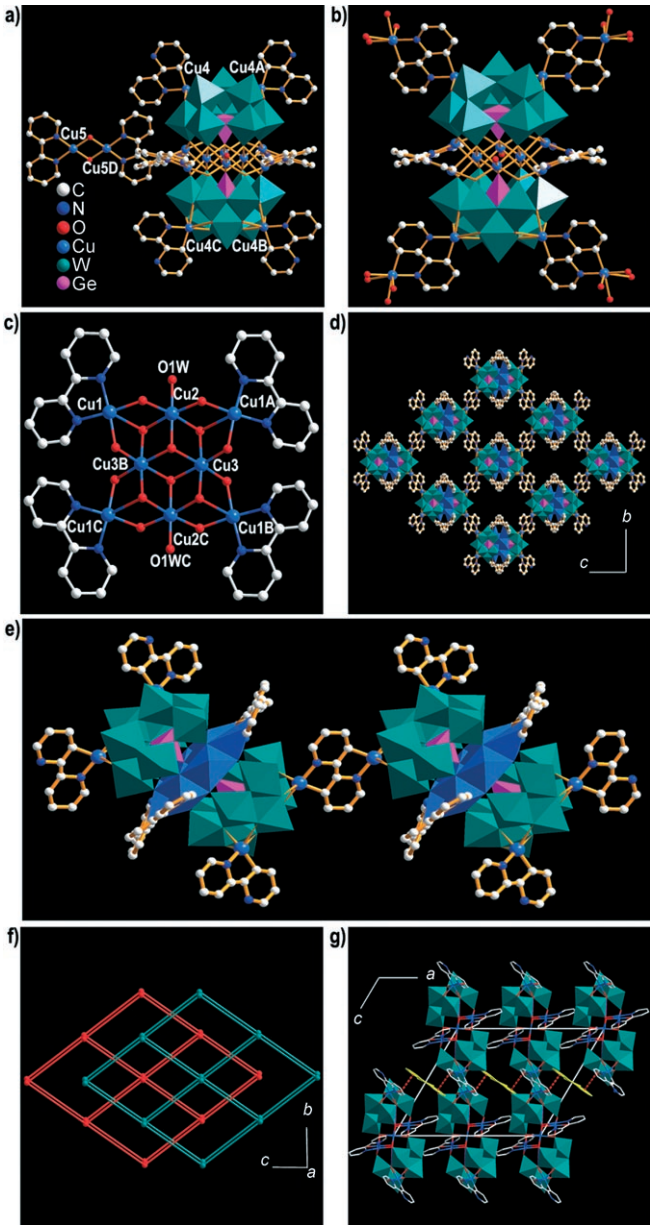

Figure 4. a) Ball-and-stick/polyhedral representation of the molecular unit of **5**. Hydrogen atoms and lattice water molecules are omitted for clarity. b) The connection fashion of $[Cu^{II}_2(bdyl)]^{2+}$ groups and the $[Cu^{II}_8(2,2'\text{-bpy})_4(H_2O)_2(B\text{-}\alpha\text{-}GeW_9O_{34})_2]^{4-}$ unit in **5**. c) The connection motif of the $\{[Cu^{II}(2,2'\text{-bpy})]_4Cu^{II}_4O_{14}(H_2O)_2\}$ cluster. Atoms with "A–D" in their labels are symmetry-generated (A: x, $1-y$, z; B: $1-x$, $1-y$, $-z$; C: $1-x$, y, $-z$; D: $-x$, $-y$, $1-z$). d) The 2D layer of **5** along the *a*-axis showing rectangular pores with sizes of 14.0×7.2 Å. The dimeric $[Cu_2(H_2O)_2(2,2'\text{-bpy})_2]^{4+}$ cations were omitted for clarity. e) The coordination environment of the $[Cu^{II}_2(bdyl)]^{2+}$ group. f) Topological view of the 2D layers along the *a*-axis showing the (4,4)-network and the -ABAB- mode. A: green, B: red; **5a** nodes: green/red balls. g) The arrangement of hybrid polyoxoanions **5a** (green) and free dimeric cations $[Cu^{II}_2(H_2O)_2(2,2'\text{-bpy})_2]^{4+}$ (yellow) exhibiting the π–π interactions between pyridyl rings. The red dashed bonds represent the π–π interactions.

1–**4**. Intriguingly, **5** exhibits four obvious structural features different from **1**–**4**. First, although the $\{[Cu(2,2'\text{-bpy})]_4Cu_4O_{14}(H_2O)_2\}$ cluster in **5** also displays the alignment

motif of 3:2:3, four five-coordinate Cu^{II} cations are stabilized by four 2,2′-bpy ligands rather than en or dap ligands (Figure 4c).

Secondly, $[Cu_2(bdyl)]^{2+}$ groups cap to the windows on the "polar" positions of **5a** to give a beautiful flower-shaped appearance. Each $[Cu_2(bdyl)]^{2+}$ group grafts to a window through three stronger μ_3-O bridges and one weaker μ_3-O bridge with Cu–O distances of 2.181(18)–2.521(21) Å. Similar grafting fashions between $[Cu(2,2'\text{-bpy})]^{2+}$ groups and lacunary Keggin units have been observed in two inorganic–organic hybrid POTs, $[Cu_5(2,2'\text{-bpy})_6(H_2O)][B\text{-}\beta\text{-}GeW_8O_{31}]\cdot 9H_2O$[18a] and $Na\{Cu(2,2'\text{-bpy})(H_2O)\}_2\{Cu(2,2'\text{-bpy})\}_2(B\text{-}\alpha\text{-}SbW_9O_{33})]\cdot 2H_2O$.[25] For example, in the latter, each $[Cu^{II}(2,2'\text{-bpy})]^{2+}$ group also grafts to a window on the "polar" position of $[B\text{-}\alpha\text{-}SbW_9O_{33}]^{9-}$ unit with Cu-O distances of three stronger μ_3-O bridges and one weaker μ_3-O bridge in the range of 2.019(7)–2.411(7) Å.[25]

Thirdly, in the 2D architecture the bdyl group acts as a twofold-deprotonated anionic N,C∧C,N ligand that forms an unique *trans*-four-coordination mode to two Cu^{II} atoms (Figure 4e). This is the first time that such rollover metalation[17] of 2,2′-bpy has been observed in a system containing a copper complex under hydrothermal conditions.

Fourthly, there is a discrete di-Cu complex cation $[Cu_2(H_2O)_2(2,2'\text{-bpy})_2]^{4+}$ in **5**, in which each Cu^{II} ion coordinates to two N atoms of a 2,2′-bpy ligand and two bridging water ligands with Cu–N and Cu–O distances of 1.975(14) and 1.936(15) Å, respectively. Although it is not possible to locate the protons of the bridging water ligands during the structure refinement, its presence is required to balance the charge of the crystal structure and can be deduced from a calculation of the bond valence sum (BVS) around the oxygen atom (BVS = 0.99 for the oxygen using only two Cu–O bonds).[26] Of particular interest is that each hybrid dimer **5a** links to adjacent four others through four $[Cu_2(bdyl)]^{2+}$ bridges to form a 2D (4,4)-network showing rectangular pores with sizes of 14.0×7.2 Å in the *bc* plane (Figure 4f), which is distinct from known sandwich-type family of TMSPs. Apart from five 2D tetra-Zn^{II}/Ni^{II} sandwiched POTs, $[Zn(enMe)_2(H_2O)]_2\{[Zn(enMe)_2]_2[Zn_4(HenMe)_2(PW_9O_{34})_2]\}\cdot 8H_2O$, $[Zn(enMe)_2(H_2O)]_4[Zn(enMe)_2]_2[(enMe)_2]\{[Zn(enMe)_2]_2[Zn_4(HSiW_9O_{34})_2]\}\{[Zn(enMe)_2(H_2O)]_2[Zn_4(HSiW_9O_{34})_2]\}]\cdot 13H_2O$,[16a] and $\{[Ni(dap)_2(H_2O)]_2[Ni(dap)_2]_2[Ni_4(Hdap)_2(B\text{-}\alpha\text{-}HXW_9O_{34})_2]\}\cdot nH_2O$ ($n=1$, X = Si^{IV}/Ge^{IV}; $n=0$, X = P^{V})[16b] reported by our lab and a 2D tetra-Ni^{II} sandwiched POT, $(NH_4)_2[Ni_4(enMe)_8(H_2O)_2Ni_4(enMe)_2(PW_9O_{34})_2]\cdot 9H_2O$, addressed by Wang et al,[14f] to the best of our knowledge, **5** is the first 2D layer architecture constructed from octa-Cu^{II} sandwiched TMSP in POM chemistry. Notice that adjacent layers are aligned in the -ABAB- mode along the *a*- axis (Figure 4f). The discrete dimeric cations $[Cu_2(H_2O)_2(2,2'\text{-bpy})_2]^{4+}$ as spacers are filled with interlayers. The 2D layer of **5** is mainly governed by the $[Cu_2(bdyl)]^{2+}$ functionality. In the 2D architecture, the bdyl group acts as a twofold-deprotonated anionic N,C∧C,N ligand bridging two Cu^{II} ions, forming a unique $[Cu_2(bdyl)]^{2+}$ unit (Cu–N: 2.03(4) and Cu–C: 1.92(3) Å) (Scheme S1 in the Supporting Information). The formation of the bdyl can be interpreted by the rollover metalation of 2,2′-bpy. The so-called "rollover" metalation of 2,2′-bpy, which entails cleavage of a C–H bond of pyridine ring, was first observed in an Ir^{III}-complex in the 1980s.[27a–c] Since then, the rollover metalation containing cyclometalated N,C species has also been discovered in a 2,2′-bpy-based Pt^{II} complex[17] and the derivatives of 2,2′-bpy, such as N-substituted 2,2′-bpyridines,[27d] 6-substituted 2,2′-bipyridines,[27e,f] and 6,6′-substituted 2,2′-bipyridines,[27g] as well as 2,2′:6′,2″-terpyridine (see Scheme S2 in the Supporting Information).[27h] In addition, the activation of C–H bonds has been invoked to explain the formation of Ar–H, and mononuclear species was isolated in a process of thermal rearrangement of $(Ar)_2Pt(bpy)$ complexes.[17] Notice that most work in this field was focused on the reactivity of the noble metal ions with derivatives of 2,2′-bpy: Ir^{III},[27a–c] Pt^{II},[17,27d–i] Pd^{II},[27j,k] and Au^{III}.[27l] Furthermore, the behaviors of the above ligands are not easily predicable, especially in the case of Pd^{II} ions, the reactions often are driven toward unexpected results, although the related results, in the case of Pt^{II} ions, have been summarized in detail.[27g] Surprisingly, no example of cyclometalated N,C species has been described in the 2,2′-bpy-based low-priced Cu^{II} complexes. Recently, it has been found that the Cu^{II} cations play a very important role in the following reactions under hydrothermal conditions, such as rearrangement reactions,[28a] oxidative hydroxylation of aromatic rings,[28b,c] dehydrogenative coupling of carbon–carbon bonds,[28d] cycloaddition of organic nitriles with azide or ammonia,[28e] transformation of inorganic, and organic sulfur,[28f,g] decarboxylation of carboxylic acids,[28h] hydrolysis of cyanopyridine,[28i] etc (Scheme S3 in the Supporting Information). Here the rollover metalation of 2,2′-bpy in the presence of Cu^{II} ions has been discovered.

From the viewpoint of topology, if the $\{[Cu(bdyl)]_2\{Cu_8(Ge\,W_9O_{34})_2\}\}$ units are considered as four-connected nodes, the 2D structure possesses a 2D (4,4)-network topology (Figure 4f), which not only enriches topological types of POMs, but also provides the guidance for development of coordination network and discovery of novel topologies in POM chemistry. Additionally, the perpendicular distances between pyridyl rings of $[Cu_2(H_2O)_2(2,2'\text{-bpy})_2]^{4+}$ cations and pyridyl rings of $[Cu_2(bdyl)]^{2+}$ bridges are ≈4.1 Å, indicating the presence of weak π–π interactions. Taking into account such weak π–π interactions, the 2D structure of **5** is extended to the 3D supramolecular architecture (Figure 4g).

Structure of $[Cu^{I}(2,2'\text{-bpy})(4,4'\text{-bpy})]_2\{[Cu^{I}_2(2,2'\text{-bpy})_2(4,4'\text{-bpy})][Cu^{I}_2Cu^{II}_6(2,2'\text{-bpy})_2(4,4'\text{-bpy})_2(B\text{-}\alpha\text{-}GeW_9O_{34})_2]\}\cdot 2H_2O$ (6): Unlike compounds **1**–**5**, compound **6** crystallizes in the triclinic space group $P\bar{1}$. The molecular structure of **6** contains a mixed-valent octa-Cu sandwiched dimer $[Cu^{I}_2Cu^{II}_6(2,2'\text{-bpy})_2(4,4'\text{-bpy})_2(B\text{-}\alpha\text{-}GeW_9O_{34})_2]^{14-}$ (**6a**), two supporting di-Cu^{I} coordination cations $[Cu^{I}_2(2,2'\text{-bpy})_2(4,4'\text{-bpy})]^{2+}$, two free mononuclear Cu^{I} cations $[Cu^{I}(2,2'\text{-bpy})(4,4'\text{-bpy})]^{+}$ and two lattice water molecules (Figure 5a). The dimer **6a** is built by two trivacant Keggin B-α-GeW_9

moieties linked by a novel octa-Cu $\{[Cu^{I}_{2}Cu^{II}_{2}(2,2'\text{-bpy})_{2}(4,4'\text{-bpy})_{2}]Cu^{II}_{4}O_{14}\}$ (**6b**) cluster. The connection motif of two B-α-GeW_9 moieties and **6b** is analogous to those in **1**–**5**. An interesting structural characteristic is that the linking mode of **6b** is quite different from those in **1**–**5**, although eight copper centers in **1**–**6** are all distributed in the fashion of 3:2:3. The unprecedented **6b** (Figure 1s, Figure 5b) is composed of two $Cu^{II}O_6$ (two Cu4) octahedra [Cu–O: 1.928(8)–2.443(12) Å], two $Cu^{II}O_5$ (two Cu2) square pyramids [Cu–O: 1.939(7)–2.260(7) Å], two $Cu^{II}O_3N_2$ (two Cu1) square pyramids [Cu–O: 1.947(7)–2.344(8) Å and Cu–N: 2.002(7)–2.011(7) Å] and two $Cu^{I}O_3N$ (two Cu_3) tetrahedra [Cu–O: 2.083(8)–2.250(8) Å and Cu–N: 1.941(7) Å], which are connected in the edge-shared fashion, whereas the octa-Cu $\{[Cu^{II}(L)]_4Cu^{II}_4O_{14}(H_2O)_2\}$ clusters (L = en/dap) in **1**–**4** are built by four $Cu^{II}O_6$ octahedra and four $Cu^{II}O_3N_2$ square pyramids, which are also combined together in the edge-shared fashion. Similarly, the mixed-valent **6a** can be also viewed as another derivative of the tetra-Cu sandwiched unit $[Cu^{II}_4(H_2O)_2(B\text{-}\alpha\text{-}GeW_9O_{34})_2]^{12-}$.[7d] Under the condition of removal of two coordinated water molecules, **6b** can be also considered that two five-coordinate $[Cu^{II}(2,2'\text{-bpy})]^{2+}$ cations and two four-coordinate $[Cu^{I}(4,4'\text{-bpy})]^{+}$ cations diagonally graft to the four corners of the rhombic $\{Cu^{II}_4O_{14}\}$ unit through twelve oxygen atoms from the lacunae of two B-α-GeW_9 fragments.

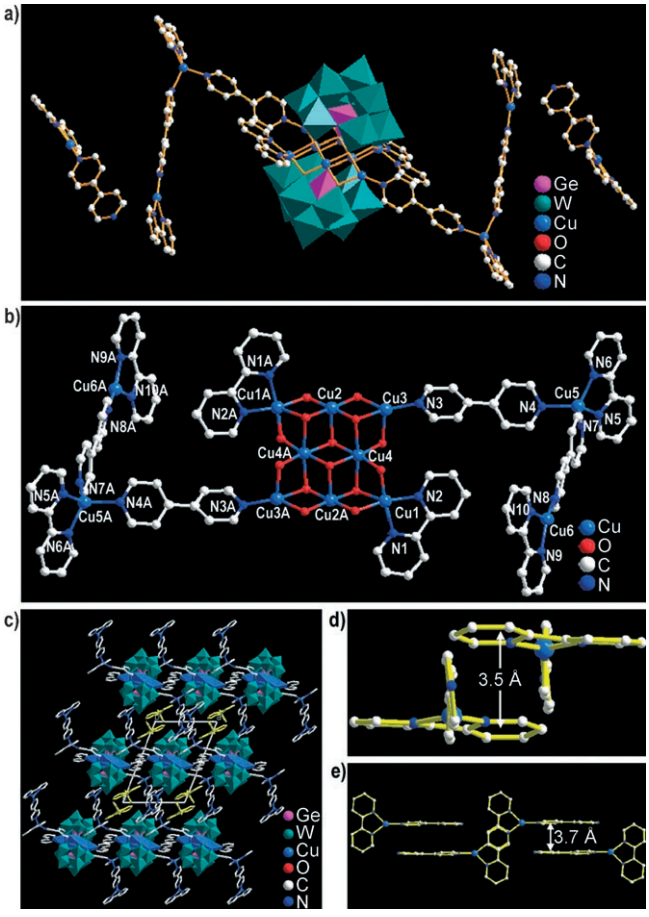

Figure 5. a) Ball-and-stick/polyhedral representation of the molecular structure of **6**. Hydrogen atoms and lattice water molecules are omitted for clarity. b) The octa-Cu cluster **6b** symmetrically connecting two di-Cu^{I} coordination cations $[Cu^{I}_{2}(2,2'\text{-bpy})_{2}(4,4'\text{-bpy})]^{2+}$ generating an unprecedented hybrid inorganic–organic dodeca-Cu cluster. Atoms with "A" in their labels are symmetry-generated (A: $1-x$, $1-y$, $1-z$). c) The packing of **6** along the *b*-axis showing parallelogram channels, in which free mononuclear Cu^{I} cations $[Cu^{I}7(2,2'\text{-bpy})(4,4'\text{-bpy})]^{+}$ are filled. The $[Cu^{I}7(2,2'\text{-bpy})(4,4'\text{-bpy})]^{+}$ cations are highlighted in yellow. d) The vertical distance between two parallel 2,2′-bpy rings is 3.5 Å. e) The vertical separation between two parallel 4,4′-bpy rings is 3.7 Å.

Another remarkable structural characteristic is that two di-Cu^{I} coordination cations $[Cu^{I}_{2}(2,2'\text{-bpy})_{2}(4,4'\text{-bpy})]^{2+}$ symmetrically link to **6b** through two 4,4′-bpy bridges, generating an unprecedented hybrid inorganic–organic dodeca-Cu cluster (Figure 5b) that can not be found in coordination chemistry stored in the Cambridge Crystallographic Data Center (CCDC). In $[Cu^{I}_{2}(2,2'\text{-bpy})_{2}(4,4'\text{-bpy})]^{2+}$ group, two Cu^{I} (Cu5, Cu6) cations are unique and both have different coordination configurations. One (Cu5) is four-coordinate $Cu^{I}N_4$ tetrahedral geometry defined by two N atoms from one 2,2′-bpy and two N atoms from two 4,4′-bpy with Cu–N distances of 2.020(9)–2.064(9) Å, the other (Cu6) is tri-coordinate $Cu^{I}N_3$ trigonal configuration constituted by two N atoms from one 2,2′-bpy and one N atoms from one 4,4′-bpy with Cu–N distances of 1.927(9)–2.070(13) Å. In addition, two $[Cu^{I}(2,2'\text{-bpy})(4,4'\text{-bpy})]^{+}$ groups adopt tri-coordinate $Cu^{I}N_3$ trigonal geometry built by two N atoms from one 2,2′-bpy and one N atom from one 4,4′-bpy with Cu–N distances of 1.896(11)–2.016(12) Å. Notably, although there are some reports on trigonal coordinate Cu^{I} complexes with cyanide ligands[29] or other mixed ligands in which the L-Cu-L angles are nearly 120°,[30] such trigonal coordination mode of Cu^{I} ions is rather rare in POM chemistry.[31] Additionally, the tri-coordinate T-shaped geometry of Cu^{I} ions was also observed.[32] Notice that there are seven unique Cu ions in **6**: three are +2 (Cu1, Cu2, and Cu4), and the rest are +1 (Cu3, Cu5, Cu6, and Cu7) that further confirmed by the bond valence sum (BVS) calculations.[26,33] The BVS values of Cu1–Cu7 are 2.09, 2.08, 1.06, 2.13, 1.17, 1.01, and 1.08, respectively, which are in good agreement with their coordination geometries. As no Cu^{I} ions were used in making **6**, the Cu^{I} ions must result from the reduction of Cu^{II} ions. It is a common phenomenon that the high oxidation state metals are reduced by bipyridine under hydrothermal conditions.[16c,30,31] For example, Wang et al. made a mixed-valent hybrid inorganic–organic POM, $[Cu^{I}_{3}Cl(4,4'\text{-bpy})_4]$-$[Cu^{II}(1,10\text{-phen})_2Mo_8O_{26}]$, in which 4,4′-bpy not only worked as a rigid ligand, but also a reducing agent.[16c]

In addition, provided that the weak C-H···O hydrogen bonding interactions between carbon atoms of bpy ligands and O atoms of B-α-GeW_9 units (C-H···O: 2.975(13)–3.44(2) Å) are considered, thus, the 3D supramolecular architecture of **6** comes into being. Such weak C-H···O interactions were also observed in hybrid inorganic–organic POMs.[34] For instance, Gutiérrez-Zorrilla et al used the d_e Hirshfeld surface to depict C-H···O weak interactions between phenanthroline aromatic rings and POM surface O atoms.[34a] The packing of **6** along the *b*-axis exhibits paral-

lelogram channels, in which $[Cu^{I}7(2,2'\text{-bpy})(4,4'\text{-bpy})]^{+}$ cations are filled (Figure 5c). In the channels, adjacent pyridyl rings of $[Cu^{I}7(2,2'\text{-bpy})(4,4'\text{-bpy})]^{+}$ cations surround a pseudo-square window. The vertical distance between two parallel 2,2′-bpy/4,4′-bpy rings is 3.5/3.7 Å (Figure 5d,e), indicating the presence of weak π–π interactions. Therefore, the $[Cu^{I}7(2,2'\text{-bpy})(4,4'\text{-bpy})]^{+}$ cations can not only act as counteract-ions to interact with the skeletons of polyoxoanions through electro-static interactions, but also form 1D supramolecular chain by means of weak π–π interactions. These two types of interaction are responsible for stabilizing the structures.

Comparing **6** with **1**–**5**, five notable differences are observed: 1) **6** is a mixed-valent POT containing Cu^{I}/Cu^{II} cations, whereas **1**–**5** only contain Cu^{II} cations; 2) **6** contains two kinds of ligands of 2,2′-/4,4′-bpy, to our knowledge, the TMSPs with mixed ligands are rare,[31,18b] **1**–**5** only include one kind of ligand; 3) The octa-Cu $\{[Cu^{I}_2Cu^{II}_2(2,2'\text{-bpy})_2(4,4'\text{-bpy})_2]Cu^{II}_4O_{14}\}$ cluster in **6** is stabilized by two chelating 2,2′-bpy and two mono-coordinate 4,4′-bpy, whereas the octa-Cu $\{[Cu^{II}(L)]_4Cu^{II}_4O_{14}(H_2O)_2\}$ clusters in **1**–**5** are stabilized by four identical didentate ligands (L = en, dap, 2,2′-bpy); 4) The $\{[Cu^{I}_2Cu^{II}_2(2,2'\text{-bpy})_2(4,4'\text{-bpy})_2]Cu^{II}_4O_{14}\}$ cluster in **6** is built by two $Cu^{II}O_6$ octahedra, two $Cu^{I}O_3N$ tetrahedra, two $Cu^{II}O_5$ and two $Cu^{II}O_3N_2$ square pyramids, whereas all the octa-Cu $\{[Cu^{II}(L)]_4Cu^{II}_4O_{14}(H_2O)_2\}$ clusters in **1**–**5** are constituted by four $Cu^{II}O_6$ octahedra and $Cu^{II}O_3N_2$ square pyramids; 5) In **6**, two di-Cu^{I} coordination cations $[Cu^{I}_2(2,2'\text{-bpy})_2(4,4'\text{-bpy})]^{2+}$ symmetrically link to the octa-Cu $\{[Cu^{I}_2Cu^{II}_2(2,2'\text{-bpy})_2(4,4'\text{-bpy})_2]Cu^{II}_4O_{14}\}$ cluster through two 4,4′-bpy bridges forming a novel dodeca-Cu cluster, whereas no such phenomenon exists in **1**–**5.**

Magnetic properties: The nonmagnetic polyoxoanion frameworks not only guarantee an effective magnetic isolation of in situ formed TM clusters, providing good opportunity for investigating magnetic exchange interactions and electron delocalization in highly symmetrical clusters, but also can control the magnitude of magnetic couplings.[1d,11,35] Of particular interest is to probe their magnetic properties of **1**–**5**, because all contain a well-isolated octa-Cu^{II} cluster sandwiched by two nonmagnetic fragments, although their structures possess some differences. Here, the magnetic properties of **1**, **4**, and **5** are investigated. In order to quantitatively describe magnetic exchange interactions within octa-Cu^{II} clusters, all the magnetic analyses are subjected to a theoretical model as shown in Figure 6a giving four exchange pathways within octa-Cu^{II} clusters.

The temperature dependence of magnetic susceptibility data for **4** is shown in Figure 7 in the form of χ_M and $\chi_M T$ versus T. The χ_M slowly increases from 0.01 emu mol^{-1} at 300 K to 0.13 emu mol^{-1} at 30 K, then exponentially to the maximum of 1.28 emu mol^{-1} at 2 K. The $\chi_M T$ of 3.25 emu mol^{-1} K at 300 K is in good agreement with the value expected for eight noncorrelated Cu^{II} ions (3.31 emu mol^{-1} K, with $g = 2.1$). As the temperature is lowered, the $\chi_M T$ increases slowly and then reaches a maximum value of

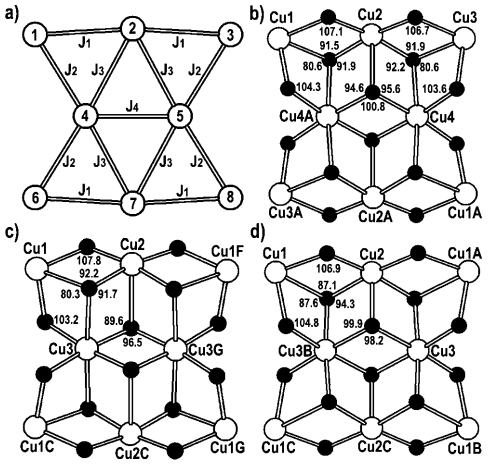

Figure 6. a) The magnetic exchange model used for the octa-copper^{II} clusters in **1**, **4** and **5**. b–d) Comparison of the Cu-O-Cu angles of the octa-copper^{II} clusters in **1**, **4** and **5**, respectively.

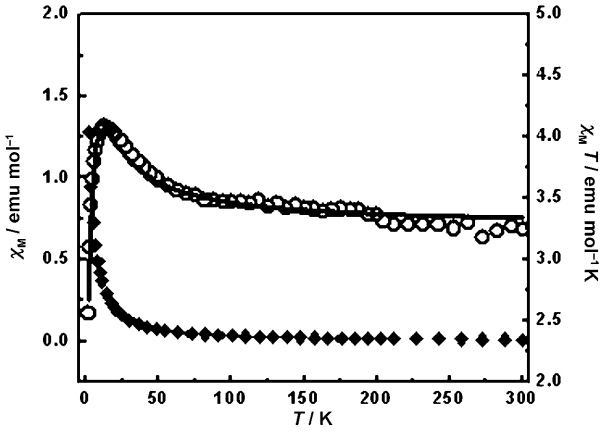

Figure 7. The plots of χ_M and $\chi_M T$ *vs* T in the temperature of 2–300 K for **1**. The solid line represents the fit to experimental data.

4.08 emu mol^{-1} K at 13 K. This behavior demonstrates dominant ferromagentic interactions among magnetic centers.[36] The sharp drop in the $\chi_M T$ value below apex temperature can be attributed to antiferromagnetic interactions, which has been proved by the theoretical simulation (vide infra). The magnetic interactions between nearest magnetic neighbors are evaluated by employing the Curie–Weiss equation $[\chi_M = C/(T-\theta)]$, which gives values of $C = 3.24$ emu mol^{-1} K and $\theta = 4.49$ K (Figure S3 in the Supporting Information). The positive Weiss constant also supports dominant ferromagnetic interactions within Cu^{II} centers mediated by oxygen bridges.

According to the C_2 symmetry of the octa-Cu^{II} cluster in **1** and structural parameters of single-crystal structural analysis (Figure 6b), we suppose that magnetic exchange interactions between Cu1···Cu2, Cu2···Cu3, Cu1 A···Cu2 A and Cu2 A···Cu3 A are equal. On this assumption, there exist four exchange constants in the octa-Cu^{II} cluster. The vertices with numbers 1, 2, 3, 4, 5, 6, 7, and 8 stand for Cu1, Cu2,

Cu3, Cu4A, Cu4, Cu3A, Cu2A, and Cu1A, respectively. The interactions between Cu1···Cu2, Cu2···Cu3, Cu3A···Cu2A, and Cu2A···Cu1A are given by the exchange constant J_1; the interactions between Cu1···Cu4A, Cu3···Cu4, Cu4A···Cu3A, and Cu4···Cu1A are given by the exchange constant J_2; the interactions between Cu2···Cu4A, Cu2···Cu4, Cu2A···Cu4A, and Cu2A···Cu4 are given by the exchange constant J_3; and the interaction between Cu4···Cu4A is given by the exchange constant J_4. Since second- and third-neighbor exchange interactions between Cu^{II} centers with significantly long distances (more than 5.5 Å) in the octa-Cu^{II} cluster are very weak, enough to be negligible, only first-neighbor exchange interactions will be considered. The magnetic behavior of **1** is analyzed by the MAGPACK program package[37] based on the isotropic Heisenberg spin Hamiltonian in Equation (1):

$$\begin{aligned} H = & -2J_1(S_1S_2 + S_2S_3 + S_6S_7 + S_7S_8) \\ & -2J_2(S_1S_4 + S_3S_5 + S_4S_6 + S_5S_8) \\ & -2J_3(S_2S_4 + S_2S_5 + S_4S_7 + S_5S_7) \\ & -2J_4S_4S_5 \end{aligned} \quad (1)$$

Substitution of the eigenvalues of Equation (1) into the standard Van Vleck equation yields the expression of molar magnetic susceptibility (χ_c) of the octa-Cu^{II} cluster, as shown in Equation (2):[38]

$$\chi_c = \frac{Ng^2\beta^2}{3kT} \cdot \frac{\{\sum S_n{}^T(S_n{}^T+1)(2S_n{}^T+1)\exp[-E_n kT]\}}{\{\sum (2S_n{}^T+1)\exp[-E_n/kT]\}} \quad (2)$$

Here, N is the Avogadro number, k is the Boltzmann constant, T is the temperature in Kelvin, and E_n is the spin exchange energy associated with a spin state $S_n{}^T$.

A molecular field approximation[39] was applied to Equation (2) to account for the intermolecular interactions (zJ') to produce Equation (3):

$$\chi_M = \frac{\chi_c}{(1-2zJ'\chi_c/Ng^2\beta^2)} \quad (3)$$

The best fit of the experimental data in the overall temperature range is shown in Figure 7 with $J_1 = -4.03\ cm^{-1}$, $J_2 = 3.80\ cm^{-1}$, $J_3 = 8.58\ cm^{-1}$, $J_4 = 0.12\ cm^{-1}$, $g = 2.09$, and $zJ' = 0\ cm^{-1}$. The agreement factor R, defined as $\Sigma[(\chi_M)_{obs} - (\chi_M)_{cal}]^2/\Sigma(\chi_M)_{obs}{}^2$, is equal to 2.34×10^{-4}. Simulation results manifest that the contribution from the intercluster magnetic interactions could be negligible since $zJ' = 0\ cm^{-1}$. The ferromagnetic and antiferromagnetic exchange constants obtained by this analysis approximately conform to the correlation between the experimental exchange constants and the Cu-O-Cu bond angles that is concluded from extensive experimental and theoretical studies performed on the spin exchanges within $[Cu_2O_2]$ units constituted by hydroxide[40a] and alkoxide[40b–c] bridges. It is clear from this vast amount research that the nature and strength of the exchange are chiefly affected by the Cu-O-Cu bond angles (Φ). The classical correlation between the exchange constants and the Cu-O-Cu bond angles indicates that the complexes are generally antiferromagnetic for $\Phi > 98°$, whereas ferromagnetic for $\Phi < 98°$.[40d–f] The Cu-O-Cu angles vary from 80.6 to 107.1° in **1**, thus competitive ferromagnetic and antiferromagnetic interactions are expected. The field dependence of magnetization reveals that the magnetization curve at 2 K increases with raising applied field, but its value stays smaller than the theoretical value calculated from the Brillouin function for eight uncoupled Cu^{II} spins (Figure 8). Such behavior can suggest the coexistence of ferromagnetic interactions ($J_2 > 0$, $J_3 > 0$, and $J_4 > 0$) and antiferromagnetic interactions ($J_1 < 0$) in the structure. This explanation is also ascertained by the fact that the maximum of the $\chi_M T$ value of 4.08 emu mol^{-1} K at 13 K is far smaller than the theoretical expected value of 11.03 emu mol^{-1} K (considering $g = 2.1$) for the ferromagnetic octa-Cu^{II} cluster mediated by oxygen bridges. This phenomenon of coexistence of ferromagnetic and antiferromagnetic exchanges between Cu^{II} centers has been observed in $K_7Na[Cu_4K_2(H_2O)_6(\alpha\text{-}AsW_9O_{33})_2]\cdot 5.5H_2O$.[20]

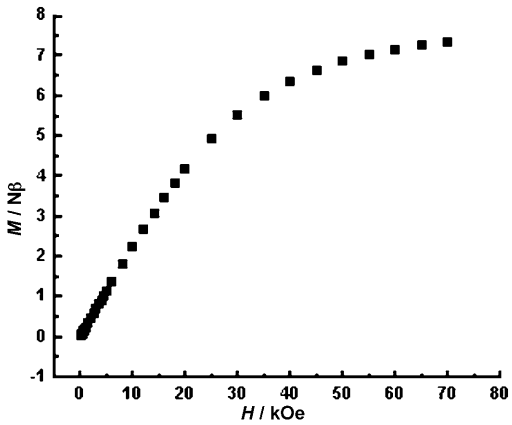

Figure 8. The filed dependence of magnetization for **1** at 2 K.

The temperature dependence of magnetic susceptibility data for **4** is shown in Figure 9 in the form of χ_M and $\chi_M T$ versus T. The $\chi_M T$ value corresponds to 3.39 emu mol^{-1} K at 300 K, which is in good consistence with the spin-only contribution (3.38 emu mol^{-1} K) expected for nine isolated Cu^{II} ($S = 1/2$) ions assuming $g = 2$ per formula unit. Upon cooling, the $\chi_M T$ product experiences a gradual rise and reaches a maximum value of 8.52 emu mol^{-1} K at 8 K. This behavior indicates ferromagnetic interactions within Cu^{II} centers. A sharp drop below the cusp temperature is observed, designating that prevalent antiferromagnetic interactions are operative. The inverse magnetic susceptibility data in 2–300 K are fitted with the Curie–Weiss equation, providing parameters of $C = 3.35$ emu mol^{-1} K and $\theta = 12.54$ K (Figure S4a in the Supporting Information). The larger positive Weiss constant (θ) suggests that individual Cu^{II} spins interact stronger ferromagnetically in the lattice.

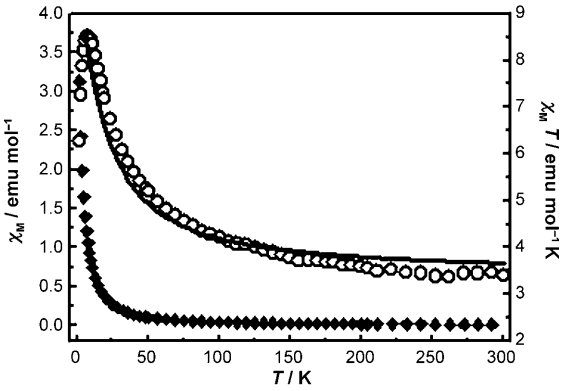

Figure 9. The plots of χ_M and $\chi_M T$ *vs* T in the temperature of 2–300 K for **4**. The solid line represents the fit to experimental data.

Since the octa-Cu^{II} cluster in **4** employs the C_4 symmetry, there are four types of Cu···Cu distances: 3.15 Å (Cu1···Cu2), 3.09 Å (Cu1···Cu3), 3.16 Å (Cu2···Cu3), and 2.93 Å (Cu3···Cu3B) and seven types of Cu-O-Cu angles: 107.8° (Cu1-O16-Cu2), 92.2° (Cu1-O9C-Cu2), 80.3° (Cu1-O9C-Cu3), 103.2° (Cu1-O12-Cu3), 91.7° (Cu2-O9C-Cu3), 89.6° (Cu2-O20-Cu3), and 96.5° (Cu3-O20-Cu3B). Thus, the magnetic property of **4** can be analyzed by magnetic exchange model as shown in Figure 6a. The vertices with numbers 1, 2, 3, 4, 5, 6, 7, and 8 symbolize Cu1, Cu2, Cu1F, Cu3, Cu3G, Cu1C, Cu2C, and Cu1G, respectively. The interactions between Cu1···Cu2, Cu2···Cu1F, Cu1C···Cu2C, and Cu2C···Cu1G are defined by the exchange constant J_1; the interactions between Cu1···Cu3, Cu1F···Cu3G, Cu1C···Cu3, and Cu1G···Cu3G are defined by the exchange constant J_2; the interactions between Cu2···Cu3, Cu2···Cu3G, Cu2C···Cu3, and Cu2C···Cu3G are defined by the exchange constant J_3 and the interaction between Cu3···Cu3G is defined by the exchange constant J_4. In the presence of an external magnetic field, the isotropic spin Hamiltonian of the octa-Cu^{II} cluster is given in Equation (1).

Considering the paramagnetic bridging $[Cu4(H_2O)_2]^{2+}$ ion, the paramagnetic contribution of $[Cu4(H_2O)_2]^{2+}$ ion is added to Equation (2), which leads to the expression of the molar magnetic susceptibility (χ) of **4**:

$$\chi = \chi_c + \frac{(^1/_2)(^3/_2)Ng^2\beta^2}{3kT} \quad (4)$$

Here, the second term refers to the susceptibility of a paramagnetic Cu^{II} contribution. To assess intercluster magnetic interaction (zJ'), the molecular field correction is incorporated into the magnetic model. A more general computational method has been used for this system, such as MAGPACK program package.[37] A best fit of the experimental data in the temperature range of 8–300 K affords magnetic parameters of $J_1 = -1.28\ cm^{-1}$, $J_2 = 17.10\ cm^{-1}$, $J_3 = 16.22\ cm^{-1}$, $J_4 = 15.34\ cm^{-1}$, $g = 2.11$, $zJ' = -0.03\ cm^{-1}$ and $R = 8.32 \times 10^{-3}$. These coupling constants confirm the existence of stronger ferromagnetic interactions within Cu^{II} centers.

The field dependence of magnetization (Figure S4b in the Supporting Information) reveals that the magnetization curve at 2 K increases with raising applied field, but its value stays slightly smaller than the theoretical value calculated from the Brillouin function for uncoupled nine Cu^{II} spins. Such phenomenon may suggest that ferromagnetic interactions ($J_2 > 0$, $J_3 > 0$, and $J_4 > 0$) coexist with antiferromagnetic interactions ($J_1 < 0$) in the structure, which is further consolidated by the fact that the maximum of the $\chi_M T$ value of 8.52 emu mol^{-1} K at 8 K is smaller than the theoretical expected value of 13.64 emu mol^{-1} K ($g = 2.1$) for ferromagnetic octa-Cu^{II} cluster through oxygen bridges and one isolated paramagnetic Cu^{II} ion. Notably, ferromagnetic interactions within Cu^{II} centers in **4** are stronger than those in **1**, the main reason for which can be explained as follows: Although both contain an octa-Cu^{II} cluster in their structures, their structural parameters and symmetries are somewhat different (Figure 6b,c). In **1**, the B-α-GeW_9 fragment imposes its geometry to the in situ formed octa-Cu^{II} cluster, whereas in **4**, the B-α-SiW_9 fragment also imposes its geometry to the in situ formed octa-Cu^{II} cluster. As we know, the atomic radius of the Ge atom is larger than that of the Si atom, which leads to the geometrical differences of B-α-GeW_9 and B-α-SiW_9 fragments. The geometrical differences impose to the octa-Cu^{II} cluster and further result in their magnetic differences. The magnetic differences between **1** and **4** prove that the nonmagnetic polyoxoanion frameworks can control the magnitude of magnetic couplings.[11,35]

Variable-temperature magnetic susceptibility for **5** was measured in the temperature range 2–300 K at a constant magnetic field of 10 kOe. The temperature dependence of χ_M and $\chi_M T$ is shown in Figure 10. The value of χ_M slowly increases from 0.02 emu mol^{-1} at 300 K to 0.12 emu mol^{-1} at 40 K, then exponentially to the maximum of 1.56 emu mol^{-1} at 2 K. At 300 K, the $\chi_M T$ value is equal to 5.13 emu mol^{-1} K, which is slightly larger than the spin-only value (4.96 emu mol^{-1} K) expected for twelve uncoupled Cu^{II} ions assuming $g = 2.1$. Upon cooling until 40 K, the $\chi_M T$ value shows a slight decrease. Below 40 K, the $\chi_M T$ value decreases rapidly with further cooling, reaching the minimum of 3.13 emu mol^{-1} K at 2 K. Such magnetic behavior is

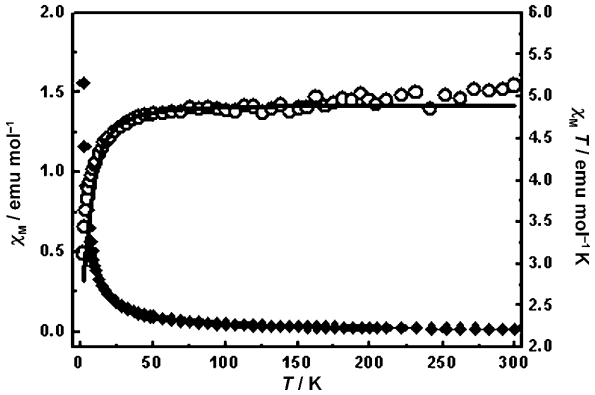

Figure 10. The plots of χ_M and $\chi_M T$ *vs* T in the temperature of 2–300 K for **5**. The solid line represents the fit to experimental data.

characteristic of antiferromagnetic interactions within Cu^{II} centers. Fit the magnetic susceptibility data between 2 and 300 K to the Curie–Weiss expression affording Curie constant $C = 5.08\ emu\ mol^{-1}\ K$ and Weiss constant $\theta = -3.29\ K$ (Figure S5 in the Supporting Information). The negative Weiss constant confirms existence of antiferromagnetic interactions within Cu^{II} centers.

The magnetic exchange model of the octa-Cu^{II} cluster in **5** is very similar to that in **4**, the vertices with numbers 1, 2, 3, 4, 5, 6, 7, and 8 symbolize Cu1, Cu2, Cu1A, Cu3B, Cu3, Cu1C, Cu2C, and Cu1B, respectively. The interactions between Cu1···Cu2, Cu2···Cu1A, Cu1C···Cu2C, and Cu2C···Cu1B are defined by the exchange constant J_1; ?the interactions between Cu1···Cu3B, Cu1A···Cu3, Cu1C···Cu3B, and Cu1B···Cu3 are defined by the exchange constant J_2; the interactions between Cu2···Cu3B, Cu2···Cu3, Cu2C···Cu3B, and Cu2C···Cu3 are defined by the exchange constant J_3, and the interaction between Cu3···Cu3B is defined by the exchange constant J_4. In the free di-Cu^{II} complex cation $[Cu^{II}_2(H_2O)_2(2,2'\text{-bpy})_2]^{4+}$, the interaction between Cu5···Cu5D is defined by the exchange constant J_5. In the octa-Cu^{II} cluster of **5**, four types of Cu···Cu distances are present: 3.38 Å (Cu1···Cu2), 3.28 Å (Cu1···Cu3B), 3.14 Å (Cu2···Cu3B), and 3.23 Å (Cu3···Cu3B) and seven types of Cu-O-Cu angles are shown in Figure 6d. In the di-Cu^{II} complex cation $[Cu^{II}_2(H_2O)_2(2,2'\text{-bpy})_2]^{4+}$, the Cu5···Cu5D distance and the Cu-O-Cu bond angle are 2.90 Å and 97.2°, respectively. The isotropic Heisenberg spin Hamiltonian of the magnetic behavior of the octa-Cu^{II} $\{[Cu^{II}(2,2'\text{-bpy})]_4Cu^{II}_4O_{14}(H_2O)_2\}$ cluster and the free di-Cu^{II} complex cation $[Cu^{II}_2(H_2O)_2(2,2'\text{-bpy})_2]^{4+}$ can be approximated by only first-neighbor interactions given by Equation (5):

$$\begin{aligned} H = & -2J_1(S_1S_2 + S_2S_3 + S_6S_7 + S_7S_8) \\ & -2J_2(S_1S_4 + S_3S_5 + S_4S_6 + S_5S_8) \\ & -2J_3(S_2S_4 + S_2S_5 + S_4S_7 + S_5S_7) \\ & -2J_4S_4S_5 - 2J_5S_9S_{10} \end{aligned} \quad (5)$$

The pendant [Cu4(bdyl)] groups are treated as paramagnetic ions and the similar method to **4** was adopted. All calculations were performed using the MAGPACK package.[37] A good fit with this magnetic susceptibility leads to the following magnetic parameters: $J_1 = -5.15\ cm^{-1}$, $J_2 = 2.51\ cm^{-1}$, $J_3 = 0.62\ cm^{-1}$, $J_4 = -4.01\ cm^{-1}$, $J_5 = 6.55\ cm^{-1}$, $g = 2.11$, $zJ' = 0\ cm^{-1}$, and the agreement factor $R = 1.29 \times 10^{-3}$, which confirms the overall antiferromagnetic coupling interactions in **5**. Such dominance of antiferromagnetic couplings in the polynuclear Cu^{II} complexes has been already observed.[2e,41e] Compare **5** with **1** and **4**, their magnetic differences may be related to the variation of Cu-O-Cu bond angles (Figure 6b–d).

Thermogravimetric analysis (TGA): The thermal stability was investigated on the crystalline samples under air atmosphere for **1**–**3**, and **5** from 30 to 800 °C. For **6**, in order to prevent the oxidation of Cu^{I} ions, its TG curve was performed under nitrogen atmosphere from 30 to 1000 °C. The thermogravimetric processes of **1**–**3**, and **5** are very similar and reveal two steps of slow weight loss in the range of 30–800 °C. For **1**, in the range of 30–280 °C, the weight loss of 4.31 % is caused by the loss of thirteen lattice water molecules (calcd 4.16 %), after 280 °C, a gradual weight loss of 7.60 % until 800 °C is approximately attributable to the removal of four dap ligands, two coordinated water molecules and the dehydration of four protons (calcd 6.56 %). For **2**, the first weight loss of 2.63 % between 30 and 178 °C is assigned to the release of five lattice water and two coordinated water molecules (calcd 2.31 %). The second weight loss of 6.91 % between 178 and 800 °C corresponds to the removal of six en ligands and the dehydration of four protons (calcd 7.26 %). For **3**, the first weight loss of 3.39 % from 30 to 270 °C is assigned to the release of eight lattice water and two coordinated water molecules (calcd 3.30 %), followed by a weight loss of 6.69 % approximately corresponding to the loss of six en ligands and the dehydration of four protons from 270 to 800 °C (calcd 7.20 %). For **5**, in the range 30–103 °C, the first weight loss occurs (1.83 %), corresponding well to the release of four lattice water and two coordinated water molecules (calcd 1.62 %). The second weight loss from 103 to 800 °C (18.62 %) corresponds to the decomposition of six 2,2′-bpy and two bdyl ligands and the dehydration of two protons and two hydroxyl groups (calcd 19.18 %). For **6**, the TGA curve indicates that the weight loss can be divided into three steps. The first weight loss is 0.75 % from 40 to 104 °C, corresponding to the release of two lattice water molecules (calcd 0.48 %). The combined weight loss of the second and third steps is 28.43 % between 104 and 1000 °C, assigned to the removal of eight 2,2′-bpy and six 4,4′-bpy ligands (calcd 28.56 %).

Conclusion

In this work, we have shown that the hydrothermal reaction of Cu^{II}, A-α-GeW_9/A-α-SiW_9 with didentate N-ligands (en, dap, 2,2′-bpy) can afford a family of novel hybrid inorganic–organic octa-Cu^{II} sandwiched POTs (**1**–**5**), realizing the assembly from discrete fragments, 2D sheet to 3D frameworks in sandwich-type TMSP chemistry. The successful syntheses of these POTs not only further testify that the combination of lacunary POM precursors and hydrothermal technique is a quite effective strategy in making novel hybrid inorganic–organic TMSPs, but also validate our consideration that the lacunary sites of lacunary POM fragments can function as structure-directing agents to induce larger TM oligomers, as well as the didentate N-ligands as structure-stabilizing agents to capture and stabilize in situ generated TM oligomers to construct novel and unique POTs under hydrothermal conditions.[15a–c] Alternatively, a mixture of $CuCl_2{\cdot}2H_2O$, GeO_2, $Na_2WO_4{\cdot}2H_2O$, $H_2SiW_{12}O_{40}{\cdot}2H_2O$, 2,2′-bpy, and 4,4′-bpy under hydrothermal conditions led to another unprecedented hybrid inorganic–organic mixed-valent octa-Cu sandwiched POT **6**, however, to date, **6** can not be obtained by the similar method to **1**–**5**. The systematic exploration is in

progress. To our knowledge, **1–8** represent the first family of hybrid inorganic–organic octa-Cu sandwiched POTs in POM chemistry. Interestingly, the rollover metalation of 2,2′-bpy in the presence of low-priced Cu^{II} cations has been observed under hydrothermal conditions. The magnetic properties of **1**, **4**, and **5** have been preliminary studied. Experimental results have proved that the bulky nonmagnetic poly-oxoanion frameworks can control the magnitude of magnetic couplings. On the other hand, the flexible coordination modes and obvious Jahn–Teller distortion of Cu^{II} ions provide a significant probability of constructing high-nuclear copper clusters, and continuous work is in progress in our lab. In addition, in order to obtain other novel poly-(TMSPs), besides trivacant Keggin POM precursors, tri-/hexa-vacant Dawson POM precursors have also been introduced to this system. We are currently working on the reactivity of these POM precursors with other transition metals or rare earth metals.

Experimental Section

The trilacunary Keggin polyoxoanion precursors $K_8Na_2[A\text{-}\alpha\text{-}GeW_9O_{34}]\cdot 25H_2O$,[10d] $K_{10}[A\text{-}\alpha\text{-}SiW_9O_{34}]\cdot 25H_2O$[3f] and $Na_9[A\text{-}\alpha\text{-}PW_9O_{34}]\cdot 7H_2O$[3e] were synthesized as previously described. All other chemicals were used as purchased without purification.

Synthesis of $H_4[Cu^{II}_8(dap)_4(H_2O)_2(B\text{-}\alpha\text{-}GeW_9O_{34})_2]\cdot 13H_2O$ (1): $K_8Na_2[A\text{-}\alpha\text{-}GeW_9O_{34}]\cdot 25H_2O$ (0.246 g, 0.08 mmol), $CuCl_2\cdot 2H_2O$ (0.213 g, 1.25 mmol), dap (0.10 mL, 1.178 mmol) were successively dissolved in H_2O (5 mL, 278 mmol), and then K_2CO_3 (2 M, 0.05 mL) was added (the starting pH_s 4.0). The resulting mixture was stirred for 1.5 h, sealed in a Teflon-lined steel autoclave (20 mL), kept at 100 °C for 5 days and then cooled to room temperature (the end pH_e 3.6). Dark green prismatic crystals were obtained by filtering, washed with distilled water and dried in air. Yield: ≈40 %. Elemental analysis calcd (%): C 2.56, H 1.33, N 1.99; found: C 2.74, H 1.40, N 2.03; IR(KBr pellet): 3435(vs), 3286(s), 3221(m), 2965(w), 1628(s), 1583 (m), 1458(w), 1386(w), 1193(w), 1128(w), 1060(m), 1024(m), 939(vs), 887(vs), 778(vs), 714(vs), 508(m), 452 cm^{-1} (m).

Synthesis of $(H_2en)_2[Cu^{II}_8(en)_4(H_2O)_2(B\text{-}\alpha\text{-}GeW_9O_{34})_2]\cdot 5H_2O$ (2): $K_8Na_2[A\text{-}\alpha\text{-}GeW_9O_{34}]\cdot 25H_2O$ (0.246 g, 0.08 mmol), $CuCl_2\cdot 2H_2O$ (0.213 g, 1.25 mmol), en (0.05 mL, 0.740 mmol) were successively dissolved in H_2O (5 mL, 278 mmol) (pH_s 4.0). The resulting mixture was stirred for 1 hour, sealed in a Teflon-lined steel autoclave (20 mL), kept at 100 °C for 5 days and then cooled to room temperature (pH_e 3.5). Dark green prismatic crystals were obtained by filtering, washed with distilled water and dried in air. Yield: ≈31 %. Elemental analysis calcd (%): C 2.20, H 1.22, N 2.57; found: C 2.14, H 1.50, N 2.49; IR(KBr pellet): 3424(vs), 3309(s), 3229(m), 1618(s), 1578 (m), 1508(w), 1458(w), 1277(w), 1132(w), 1098(w), 1051(m), 942(vs), 878(vs), 774(vs), 710(vs), 508(m), 455 cm^{-1} (m).

Synthesis of $[H_2en]_2[Cu^{II}_8(en)_4(H_2O)_2(B\text{-}\alpha\text{-}SiW_9O_{34})_2]\cdot 8H_2O$ (3): $K_{10}[A\text{-}\alpha\text{-}SiW_9O_{34}]\cdot 25H_2O$ (0.297 g, 0.097 mmol), $CuCl_2\cdot 2H_2O$ (0.170 g, 0.10 mmol), en (0.05 mL, 0.740 mmol) were successively dissolved in H_2O (5 mL, 278 mmol), and then K_2CO_3 (2 M, 0.05 mL) was added (pH_s 4.4). The resulting mixture was stirred for 1.5 h, sealed in a Teflon-lined steel autoclave (20 mL), kept at 100 °C for 5 days and then cooled to room temperature (pH_e 3.7). Dark green prismatic crystals were obtained by filtering, washed with distilled water and dried in air. Yield: ≈33 %. Elemental analysis calcd (%): C 2.62, H 1.32, N 3.05; found: C 2.52, H 1.44, N 2.87; IR(KBr pellet): 3447(vs), 3310(m), 3258(w), 1599(s), 1458(w), 1394(w), 1354(w), 1277(w), 1172(w), 1100(w), 1044 (m), 1008(m), 947(s), 899(vs), 798(vs), 738(s), 706(w), 686(m), 521 cm^{-1} (m).

Synthesis of $[Cu^{II}(H_2O)_2]H_2[Cu^{II}_8(en)_4(H_2O)_2(B\text{-}\alpha\text{-}SiW_9O_{34})_2]$ (4): $K_{10}[A\text{-}\alpha\text{-}SiW_9O_{34}]\cdot 25H_2O$ (0.246 g, 0.08 mmol), $CuCl_2\cdot 2H_2O$ (0.213 g, 1.25 mmol), ethylenediamine (0.05 mL, 0.740 mmol) were successively dissolved in H_2O (5 mL, 278 mmol), and then K_2CO_3 (2 M, 0.05 mL) was added (pH_s 4.0). The resulting mixture was stirred for 5 h, sealed in a Teflon-lined steel autoclave (20 mL), kept at 100 °C for 5 days and then cooled to room temperature (pH_e 3.3). Dark green octahedral crystals were obtained by filtering, washed with distilled water and dried in air. Yield: ≈23 %. Elemental analysis calcd (%): C 1.80, H 0.79, N 2.10, Cu 10.71; W 61.97; found: C 1.72, H 0.94, N 2.04, Cu 10.21, W 61.38; IR(KBr pellet): 3451(vs), 3314(m), 3242(w), 1627(s), 1583(s), 1458(w), 1361(w), 1072(s), 951(s), 883(vs), 814(s), 722(vs), 524 cm^{-1} (m).

Synthesis of $[Cu^{II}_2(H_2O)_2(2,2'\text{-}bpy)_2]\{[Cu^{II}(bdyl)]_2[Cu^{II}_8(2,2'\text{-}bpy)_4(H_2O)_2(B\text{-}\alpha\text{-}GeW_9O_{34})_2]\}\cdot 4H_2O$ (5):

Method A: $K_8Na_2[A\text{-}\alpha\text{-}GeW_9O_{34}]\cdot 25H_2O$ (0.369 g, 0.12 mmol), $CuCl_2\cdot 2H_2O$ (0.085 g, 0.50 mmol), 2,2′-bpy (0.039 g, 0.25 mmol) and 4,4′-bpy (0.078 g, 0.50 mmol) were successively dissolved in H_2O (8 mL, 444 mmol), and then NaOH (2 M, 0.15 mL) was added (pH_s 10.1). The resulting mixture was stirred for 5 h, sealed in a Teflon-lined steel autoclave (20 mL), kept at 150 °C for 5 days and then cooled to room temperature (pH_e 7.7). Blue parallelepiped crystals were obtained by filtering, washed with distilled water and dried in air. Yield: ≈43 %.

Method B: A mixture of GeO_2 (0.016 g, 0.15 mmol), $Na_2WO_4\cdot 2H_2O$ (0.198 g, 0.60 mmol), $H_2SiW_{12}O_{40}\cdot 2H_2O$ (0.174 g, 0.06 mmol), $CuCl_2\cdot 2H_2O$ (0.026 g, 0.15 mmol), 2,2′-bpy (0.020 g, 0.13 mmol), 4,4′-bpy (0.010 g, 0.065 mmol) and H_2O (5 mL, 278 mmol) was stirred for 1 hour, and its pH value was adjusted to pH_s 9.0 using NaOH (1 M). The resulting mixture was sealed in a Teflon-lined steel autoclave (20 mL), kept at 170 °C for 5 days and then cooled to room temperature (pH_e = 8.1). Blue parallelepiped crystals were obtained by filtering, washed with distilled water and dried in air. Yield: ≈30 %. Elemental analysis calcd (%): C 14.35, H 1.14, N 3.35, Cu 11.39, W 49.43; found: C 14.50, H 1.24, N 3.60, Cu 11.43, W 49.24; IR(KBr pellet): 3447(vs), 1631(m), 1603(s), 1568(w), 1497(w), 1474(w), 1447(m), 1318(w), 1252(w), 1158(w), 1106(w), 1060(w), 1034(w), 953(vs), 889(vs), 834(vs), 777(vs), 730(vs), 708(s), 490 cm^{-1} (m).

Synthesis of $[Cu^{I}(2,2'\text{-}bpy)(4,4'\text{-}bpy)]_2\{[Cu^{I}_2(2,2'\text{-}bpy)_2(4,4'\text{-}bpy)]_2[Cu^{I}_2Cu^{II}_6(2,2'\text{-}bpy)_2(4,4'\text{-}bpy)_2(B\text{-}\alpha\text{-}GeW_9O_{34})_2]\}\cdot 2H_2O$ (6): The method is similar to the method B of **5**, only the amount of $H_2SiW_{12}O_{40}\cdot 2H_2O$ was decreased to 0.087 g (0.03 mmol) (pH_s = 9.5 and pH_e = 8.6). Finally, dark polyhedral crystals were obtained. Yield: ≈35 %. Elemental analysis calcd (%): C 21.97, H 1.53, N 5.12; found: C 21.95, H 1.50, N 5.11; IR(KBr pellet): 3441(vs), 1600(m), 1491(w), 1471(w), 1441(w), 1410(w), 1313(w), 1245 (w), 1172(w), 1104(w), 1016(w), 944(vs), 884(s), 854(s), 818(m), 773(vs), 730(s), 719 (s), 525(m), 495 cm^{-1} (m).

Physical measurements: Elemental analyses (C, H, and N) were performed by using a PE 2400 II elemental analyzer. Inductively coupled plasma (ICP) analysis was performed by means of a Jobin Yvon ultima 2 spectrometer. IR spectra were obtained by means of an ABB Bomen MB 102 spectrometer with pressed KBr pellets in the range of 4000–400 cm^{-1}. Thermo-gravimetric analyses (TGA) were performed by using a Mettler TGA/SDTA851 thermal analyzer in the flowing air atmosphere in the temperature region of 30–800 °C for **1–3**, **5** and in the flowing nitrogen atmosphere in the temperature region of 30–1000 °C for **6** with a heating rate of 10 °C min^{-1}. Magnetic susceptibility measurements were carried out by using a Quantum Design MPMS-5 magnetometer in the temperature range of 2–300 K. The susceptibility data were corrected from the diamagnetic contributions as deduced by using Pascal's constant tables.

X-Ray crystallography: A single-crystal was mounted on a glass fiber for indexing and intensity data were collected at 293 K on a Siemens Smart 1 K CCD for **1**, Rigaku Mercury 70 CCD diffractometer for **2, 3** and **6**, and Rigaku Saturn 70 CCD diffractometer for **4** and **5** with graphite-monochromated MoK_α radiation (λ = 0.71073 Å). Direct methods were used to solve the structures and to locate the heavy atoms using the SHELXTL-97 program package.[41] The remaining atoms were found from successive full-matrix least-squares refinements on F^2 and Fourier syntheses. Routine Lorentz polarization corrections and empirical absorption correction were applied to intensity data. No hydrogen atoms

associated with water molecules were located from the difference Fourier map. Hydrogen atoms attached to carbon and nitrogen atoms were geometrically placed. All hydrogen atoms were refined isotropically as a riding mode using the default SHELXTL parameters. For **1**, all non-H atoms were refined anisotropically except for the free water molecules (O3W, O4W, O6W-O10W) and two carbon atoms (C4 and C6). The C6 atom was disordered over two positions with the occupation factors of 0.6 and 0.4, respectively. For **2**, all non-H atoms were refined anisotropically except for some oxygen, free water molecules and some carbon atoms. Although the crystal quality is poor, its structure has been completely determined by X-ray diffraction. We tried many times to improve the crystal quality, however, failed. For **3**, all non-H atoms were refined anisotropically except for the free water molecules (O2W-O5W), two nitrogen atoms (N5 and N6) and two carbon atoms (C3-C5). For **4**, all non-H atoms were refined anisotropically except for two free water molecules (O2W and O3W). For **5**, Cu2, C1, C3-C10, C12, N2 and N3 atoms were also disordered over two positions. O20, O22, O1W and O2W atoms were refined isotropically and the remaining atoms were refined anisotropically. For **6**, both W6 and O7 atoms were disordered over two positions with the occupation factors of 0.9 and 0.1 for W6 and W6′, and 0.65 and 0.35 for O7 and O7′, respectively. O7, O1W, C41-C43, C48, C49, C63 and C64 atoms were refined isotropically and the remaining atoms were refined anisotropically. Crystallographic data and structure refinements for **1**–**6** are summarized in Table 2. CCDC 664128 (**1**), 664129 (**2**), 664130 (**3**), 663471 (**4**), 664132 (**5**), and 664133 (**6**) contain the supplementary crystallographic data for this paper. These data can be obtained free of charge from The Cambridge Crystallographic Data Centre via www.ccdc.cam.ac.uk/data_request/cif.

Acknowledgements

This work was supported by the National Natural Science Fund for Distinguished Young Scholars of China (no. 20725101), the 973 Program (no. 2006CB932904), the NSF of Fujian Province (no. E0510030), the Knowledge Innovation Program of CAS (no. KJCX2.YW.H01), and the NNSF of China (no. 20521101).

[1] a) M. T. Pope, *Heteropoly and Isopoly Oxometalates*, Springer-Verlag, Berlin, **1983**; b) C. L. Hill, *Chem. Rev.* **1998**, *98*, 1; c) C. L. Hill, C. M. Prosser-McCartha, *Coord. Chem. Rev.* **1995**, *143*, 407; d) J. M. Clemente-Juan, E. Coronado, *Coord. Chem. Rev.* **1999**, *193–195*, 361; e) I. V. Kozhevnikov, *Catalysts for fine chemical synthesis-Catalysis by polyoxometalates*, John Wiley and Sons, Chichester, UK, **2002**.

[2] a) T. J. R. Weakley, H. T. Evans Jr, J. S. Showell, G. F. Tourné, C. M. Tourné, *J. Chem. Soc. Chem. Commun.* **1973**, 139; b) R. G. Finke, M. W. Droege, *Inorg. Chem.* **1983**, *22*, 1006; c) K Wassermann, M. H. Dickman, M. T. Pope, *Angew. Chem.* **1997**, *109*, 1513; *Angew. Chem. Int. Ed. Engl.* **1997**, *36*, 1445; d) M. Sadakane, M. H. Dickman, M. T. Pope, *Angew. Chem.* **2000**, *112*, 3036; *Angew. Chem. Int. Ed.* **2000**, *39*, 2914; e) P. Mialane, A. Dolbecq, J. Marrot, E. Rivière, F. Sécheresse, *Angew. Chem.* **2003**, *115*, 3647; *Angew. Chem. Int. Ed.* **2003**, *42*, 3523; f) S. S. Mal, U. Kortz, *Angew. Chem.* **2005**, *117*, 3843; *Angew. Chem. Int. Ed.* **2005**, *44*, 3773; g) P. Mialane, A. Dolbecq, J. Marrot, E. Rivière, F. Sécheresse, *Chem. Eur. J.* **2005**, *11*, 1771; h) C. Dablemont, C. G. Hamaker, R. Thouvenot, Z. Sojka, M. Che, E. A. Maatta, A. Proust, *Chem. Eur. J.* **2006**, *12*, 9150; i) P. Mialane, A. Dolbecq, F. Sécheresse, *Chem. Commun.* **2006**, 3477; j) L. Lisnard, P. Mialane, A. Dolbecq, J. Marrot, J. M. Clemente-Juan, E. Coronado, B. Keita, P. D. Oliveira, L. Nadjo, F. Sécheresse, *Chem. Eur. J.* **2007**, *13*, 3525.

[3] a) N. Haraguchi, Y. Okaue, T. Isobe, Y. Matsuda, *Inorg. Chem.* **1994**, *33*, 1015; b) P. J. Domaille, *Inorganic Syntheses*, John Wiley and Sons, New York, **1990**, *27*, 101; c) A. Tézé, G. Hervé, *Inorganic Syntheses*, John Wiley and Sons, New York, **1990**, *27*, 88; d) N. H. Nsouli, B. S. Bassil, M. H. Dickman, U. Kortz, B. Keita, L. Nadjo, *Inorg. Chem.* **2006**, *45*, 3858; e) P. J. Domaille, *Inorganic Syntheses*, John Wiley and Sons, New York, **1990**, *27*, 100; f) G. Hervé, A. Tézé, *Inorg. Chem.* **1977**, *16*, 2115; g) R. G. Finke, M. W. Droege, P. J. Domaille, *Inorg. Chem.* **1987**, *26*, 3886; h) R. Contant, *Inorganic Syntheses*, John Wiley and Sons, New York, **1990**, *27*, 108; i) R. Contant, A. Tézé, *Inorg. Chem.* **1985**, *24*, 4610.

[4] C. N. Kato, A. Shinohara, K. Hayashi, K. Nomiya, *Inorg. Chem.* **2006**, *45*, 8108.

[5] a) U. Kortz, N. K. Al-Kassem, M. G. Savelieff, N. A. Al Kadi, M. Sadakane, *Inorg. Chem.* **2001**, *40*, 4742; b) L. Bi, U. Kortz, B. Keita, L. Nadjo, H. Borrmann, *Inorg. Chem.* **2004**, *43*, 8367; c) L. Huhlmann, J. Canny, R. Contant, R. Thouvenot, *Inorg. Chem.* **2002**, *41*, 3811; d) L. Ruhlmann, L. Nadjo, J. Canny, R. Contant, R. Thouvenot, *Eur. J. Inorg. Chem.* **2002**, 975; e) M. Bösing, A. Nöh, I. Loose, B. Krebs, *J. Am. Chem. Soc.* **1998**, *120*, 7252.

[6] R. G. Finke, B. Rapko, T. J. R. Weakley, *Inorg. Chem.* **1989**, *28*, 1573.

[7] a) N. Casañ-Pastor, J. Bas-Serra, E. Coronado, G. Pourroy, L. C. W. Baker, *J. Am. Chem. Soc.* **1992**, *114*, 10380; b) J. M. Clemete-Juan, E. Coronado, J. R. Galán-Mascarós, C. J. Gómez-García, *Inorg. Chem.* **1999**, *38*, 55; c) U. Kortz, S. Isber, M. H. Dickman, D. Ravot, *Inorg. Chem.* **2000**, *39*, 2915; d) U. Kortz, S. Nellutla, A. C. Stowe, N. S. Dalal, U. Rauwald, W. Danquah, D. Ravot, *Inorg. Chem.* **2004**, *43*, 2308; e) B. S. Bassil, M. H. Dickman, U. Kortz, *Inorg. Chem.* **2006**, *45*, 2394.

[8] a) T. J. R. Weakley, R. G. Finke, *Inorg. Chem.* **1990**, *29*, 1235; b) C. J. Gómez-García, J. J. Borrás-Almenar, E. Coronado, L. Ouahab, *Inorg. Chem.* **1994**, *33*, 4016; c) R. G. Finke, T. J. R. Weakley, *J. Chem. Crystallogr.* **1994**, *24*, 123; d) J. F. Kirby, L. C. W. Baker, *J. Am. Chem. Soc.* **1995**, *117*, 10010; e) N. J. Crano, R. C. Chambers, V. M. Lunch, M. A. Fox, *J. Mol. Catal. A* **1996**, *114*, 65; f) X. Zhang, D. C. Duncan, C. F. Campana, C. L. Hill, *Inorg. Chem.* **1997**, *36*, 4208; g) A. Müller, F. Peter, M. T. Pope, D. Gatteschi, *Chem. Rev.* **1998**, *98*, 239; h) W. Song, X. Wang, Y. Liu, J. Liu, H. Xu, *J. Electroanal. Chem.* **1999**, *479*, 85; i) X. Zhang, T. M. Anderson, Q. Chen, C. L. Hill, *Inorg. Chem.* **2001**, *40*, 418; j) T. M. Anderson, K. I. Hardcastle, N. Okun, C. L. Hill, *Inorg. Chem.* **2001**, *40*, 6418; k) A. J. Gaunt, I. May, D. Collison, K. T. Holman, M. T. Pope, *J. Mol. Struct.* **2003**, *656*, 101.

[9] a) S. Nellutla, J. V. Tol, N. S. Dalal, L. H. Bi, U. Kortz, B. Keita, L. Nadjo, G. A. Khitrov, A. G. Marshall, *Inorg. Chem.* **2005**, *44*, 9795; b) C. M. Tourné, G. F. Tourné, F. Zonnevijlle, *J. Chem. Soc. Dalton Trans.* **1991**, 143; c) H. Andres, J. M. Clemente-Juan, R. Basler, M. Aebersold, H.-U. Güdel, J. J. Borrás-Almenar, A. Gaita-Ariño, E. Coronado, H. Büttner, S. Janssen, *Inorg. Chem.* **2001**, *40*, 1943.

[10] a) T. Yamase, K. Fukaya, H. Nojiri, Y. Ohshima, *Inorg. Chem.* **2006**, *45*, 7698; b) Z. Zhang, Y. Li, E. Wang, X. Wang, C. Qin, H. An, *Inorg. Chem.* **2006**, *45*, 4313; c) J. Wang, P. Ma, Y. Shen, J. Niu, *Cryst. Growth Des.* **2007**, *7*, 603; d) L. Bi, U. Kortz, S. Nellutla, A. Stowe, J. V. Tol, N. S. Dalal, B. Keita, L. Nadjo, *Inorg. Chem.* **2005**, *44*, 896.

[11] J. M. Clemente-Juan, E. Coronade, A. Forment-Aliaga, J. R. Galán-Mascarós, C. Giménez-Saiz, C. J. Gómez-García, *Inorg. Chem.* **2004**, *43*, 2689.

[12] a) B. S. Bassil, U. Kortz, A. S. Tigan, J. M. Clemente-Juan, B. Keita, P. D. Oliveira, L. Nadjo, *Inorg. Chem.* **2005**, *44*, 9360; b) Z, Zhang, Y. Qi, C. Qin, Y. Li, E. Wang, X. Wang, Z. Su, L. Xu, *Inorg. Chem.* **2007**, *46*, 8162.

[13] a) I. M. Mbbomekalle, B. Keita, M. Nierlich, U. Kortz, P. Berthet, L. Nadjo, *Inorg. Chem.* **2003**, *42*, 5143; b) M. D. Ritorto, T. M. Anderson, W. A. Neiwert, C. L. Hill, *Inorg. Chem.* **2004**, *43*, 44.

[14] a) X. Fang, T. M. Anderson, C. L. Hill, *Angew. Chem.* **2005**, *117*, 3606; *Angew. Chem. Int. Ed.* **2005**, *44*, 3540; b) S.-T. Zheng, M.-H. Wang, G.-Y. Yang, *Chem. Asian J.* **2007**, *2*, 1380; c) J.-W. Zhao, B. Li, S.-T. Zheng, G.-Y. Yang, *Cryst. Growth Des.* **2007**, *7*, 2658; d) J.-W. Zhao, S.-T. Zheng, G.-Y. Yang, *J. Solid State Chem.* **2007**, *180*, 3317; e) S.-T. Zheng, D.-Q. Yuan, J. Zhang, G.-Y. Yang, *Inorg. Chem.* **2007**, *46*, 4569; f) Z. Zhang, J. Liu, E. Wang, C. Qin, Y. Li, Y. Qi, X. Wang, *Dalton Trans.* **2008**, 463; g) N. Belai, M. T. Pope,

Chem. Commun. **2005**, 5760; h) J. Wang, X. Du, J. Niu, *Chem. Lett.* **2006**, *35*, 1408.
[15] a) S.-T. Zheng, D.-Q. Yuan, H.-P. Jia, J. Zhang, G.-Y. Yang, *Chem. Commun.* **2007**, 1858; b) J.-W. Zhao, H.-P. Jia, J. Zhang, S.-T. Zheng, G.-Y. Yang, *Chem. Eur. J.* **2007**, *13*, 10030; c) J.-W. Zhao, J. Zhang, S.-T. Zheng, G.-Y. Yang, *Chem. Commun.* **2008**, 570; d) C. Pichon, A. Dolbecq, P. Mialane, J. Marrot, E. Rivière, F. Sécheresse, *Dalton Trans.* **2008**, 71; e) J.-W. Zhao, S.-T. Zheng, W. Liu, G.-Y. Yang, *J. Solid State Chem.* **2008**, *181*, 637; f) S.-T. Zheng, J. Zhang, G.-Y. Yang, *Angew. Chem.* **2008**, *120*, 3973; *Angew. Chem. Int. Ed.* **2008**, *47*, 3909; g) A. Dolbecq, J.-D. Compain, P. Mialane, J. Marrot, E. Rivière, F. Sécheresse, *Inorg. Chem.* **2008**, *47*, 3371.
[16] a) J. Gopalakrishnan, *Chem. Mater.* **1995**, *7*, 1265; b) D. Hagrman, C. Sangregorio, C. J. O'Connor, J. Zubieta, *J. Chem. Soc. Dalton Trans.* **1998**, 3707; c) H. Jin, Y. Qi, E. Wang, Y. Li, C. Qin, X. Wang, S. Chang, *Eur. J. Inorg. Chem.* **2006**, 4541; d) P. J. Hagrman, D. Hagrman, J. Zubieta, *Angew. Chem.* **1999**, *111*, 2798; *Angew. Chem. Int. Ed.* **1999**, *38*, 2638.
[17] A. C. Skapski, V. F. Sutcliffe, G. B. Young, *J. Chem. Soc. Chem. Commun.* **1985**, 609, and references therein.
[18] a) C.- M. Wang, S.-T. Zheng, G.-Y. Yang, *Inorg. Chem.* **2007**, *46*, 616; b) L. Lisnard, A. Dolbecq, P. Mialane, J. Marrot, E. Codjovi, F. Sécheresse, *Dalton Trans.* **2005**, 3913.
[19] a) U. Kortz, I. M. Mbomekalle, B. Keita, L. Nadjo, P. Berthet. *Inorg. Chem.* **2002**, *41*, 6412; b) W. H. Knoth, P. J. Domaille, R. L. Harlow. *Inorg. Chem.* **1986**, *25*, 1577.
[20] U. Kortz, S. Nellutla, A. C. Stowe, N. S. Dalal, J. van Tol, B. S. Bassil, *Inorg. Chem.* **2004**, *43*, 144.
[21] a) J. M. Lehn, *Supramolecular Chemistry*, VCH, Weinheim, **1995**; b) O. M. Yaghi, M. O'Keeffe, N. W. Ockwig, H. K. Chae, M. Eddaoudi, J. Kim, *Nature* **2003**, *423*, 705; c) C. N. R. Rao, S. Natarajan, R. Vaidhyanathan, *Angew. Chem.* **2004**, *116*, 1490; *Angew. Chem. Int. Ed.* **2004**, *43*, 1466; d) B. Moulton, M. J. Zaworotko, *Chem. Rev.* **2001**, *101*, 1629.
[22] a) E. Coronado, C. J. Gómez-García, *Chem. Rev.* **1998**, *98*, 273; b) N. Mizuno, M. Misono, *Chem. Rev.* **1998**, *98*, 199; c) Y. P. Jeannin, *Chem. Rev.* **1998**, *98*, 51; d) L. C. W. Baker, D. C. Glick, *Chem. Rev.* **1998**, *98*, 3; e) A. Dolbecq, P. Mialane, L. Lisnard, J. Marrot, F. Sécheresse, *Chem. Eur. J.* **2003**, *9*, 2914; f) J. Lu, E. Shen, M. Yuan, Y. Li, E. Wang, C. Hu, L. Xu, J. Peng, *Inorg. Chem.* **2003**, *42*, 6956; g) P. Zheng, Y. Ren, L. Long, R. Huang, L. Zheng, *Inorg. Chem.* **2005**, *44*, 1190.
[23] H. An, E. Wang, D. Xiao, Y. Li, Z. Su, L. Xu, *Angew. Chem.* **2006**, *118*, 918; *Angew. Chem. Int. Ed.* **2006**, *45*, 904.
[24] O. V. Dolomanov, A. J. Blake, N. R. Champness, M. Schröder, *J. Appl. Crystallogr.* **2003**, *36*, 1283.
[25] J.-P. Wang, P.-T. Ma, J. Li, J.-Y. Niu, *Chem. Lett.* **2006**, *35*, 994.
[26] I. D. Brown, D. Altermatt, *Acta Cryst. B* **1985**, *41*, 244.
[27] a) G. Nord, A. C. Hazell, R. G. Hazell, O. Farver, *Inorg. Chem.* **1983**, *22*, 3429; b) P. J. Spellane, R. J. Watts, C. J. Curtis, *Inorg. Chem.* **1983**, *22*, 4060; c) P. S. Braterman, G. H. Heat, A. J. Mackenzie, B. C. Noble, R. D. Peacock, L. J. Yellowlees, *Inorg. Chem.* **1984**, *23*, 3425; d) S. Dholakia, R. D. Gillard, F. L. Wimmer, *Inorg. Chim. Acta*, **1983**, *69*, 179; e) G. Minghetti, A. Doppiu, A. Zucca, S. Stoccoro, M. A. Cinellu, M. Manassero, M. Sansoni, *Chem. Br. Chem. Heterocycl. Compd. (N. Y.)* **1999**, *35*, 992; f) A. Zucca, A. Doppiu, M. A. Cinellu, S. Stoccoro, G. Minghetti, M. Manassero, *Organometallics*, **2002**, *21*, 783, and references therein; g) A. Zucca, G. L. Petretto, S. Stoccoro, M. A. Cinellu, G. Minghetti, M. Manassero, C. Manassero, L. Male, A. Albinati, *Organometallics*, **2006**, *25*, 2253, and references therein; h) A. Doppiu, G. Minghetti, M. A. Cinellu, S. Stoccoro, A. Zucca, *Organometallics*, **2001**, *20*, 1148, and references therein; i) W. A. Wickramasinghe, P. H. Bird, N. Serpone, *J. Chem. Soc. Chem. Commun.* **1981**, 1284; j) S. Stoccoro, B. Soro, G. Minghetti, A. Zucca, M. A. Cinellu, *J. Organomet. Chem.* **2003**, *679*, 1, and references therein; k) A. Zucca, M. A. Cinellu, M. V. Pinna, S. Stoccoro, G. Minghetti, M. Manassero, M. Sansoni, *Organometallics*, **2000**, *19*, 4295, and references therein; l) M. A. Cinellu, G. Minghetti, M. V. Pinna, S. Stoccoro, A. Zucca, M. Manassero, *Eur. J. Inorg. Chem.* **2003**, *12*, 2304, and references therein.
[28] a) J. Lu, B. R. Cabrera, R. Wang, J. Li, *Inorg. Chem.* **1998**, *37*, 4480; b) X.- M. Zhang, M.- L. Tong, M.- L. Gong, H. K. Lee, L. Luo, J.-H. Li, Y.-X. Tong, X.- M. Chen, *Chem. Eur. J.* **2002**, *8*, 3187, and references therein; c) Y.-Z. Zheng, M.- L. Tong, X.- M. Chen, *New J. Chem.* **2004**, *28*, 1412, and references therein; d) X.- M. Chen, M.- L. Tong, *Acc. Chem. Res.* **2007**, *40*, 162, and references therein; e) L. Cheng, W.-X. Zhang, B.-H. Ye, J.-B. Lin, X.- M. Chen, *Inorg. Chem.* **2007**, *46*, 1135, and references therein; f) X. Zhang, R. Fang, H. Wu, *J. Am. Chem. Soc.* **2005**, *127*, 7670, and references therein; g) J. Wang, S. Zheng, M. Tong, *Inorg. Chem.* **2007**, *46*, 795, and references therein; h) Y.-Q. Sun, J. Zhang, G.-Y. Yang, *Chem. Commun.* **2006**, 1947, and references therein; i) M. Tong, L. Li, K. Mochizuki, H. Chang, X. Chen, Y. Li, S. Kitagawa, *Chem. Commun.* **2003**, 428, and references therein.
[29] a) C. Kappenstein, R. P. Hugel, *Inorg. Chem.* **1977**, *16*, 250; b) S. Lopez, S. W. Keller, *Inorg. Chem.* **1999**, *38*, 1883; c) C. Kappenstein, R. P. Hugel, *Inorg. Chem.* **1978**, *17*, 1945.
[30] K. T. Potts, C. P. Horwitz, A. Fessak, M. Keshavarz-K, K. E. Nash, P. J. Toscano, *J. Am. Chem. Soc.* **1993**, *115*, 10444.
[31] X. Kong, Y. Ren, P. Zheng, Y. Long, L. Long, R. Huang, L. Zheng, *Inorg. Chem.* **2006**, *45*, 10702.
[32] a) W. Yang, C. Lu, H. Zhuang, *J. Chem. Soc. Dalton Trans.* **2002**, 2879; b) H. Jin, Y. Qi, D. Xiao, X. Wang, S. Chang, E. Wang, *J. Mol. Struct.* **2007**, *837*, 23.
[33] a) H. H. Htorp, *Inorg. Chem.* **1992**, *31*, 1585; b) N. E. Brese, M. O'Keeffe, *Acta Cryst. B* **1991**, *47*, 192.
[34] a) S. Reinoso, P. Vitoria, L. S. Felices, L. Lezama, J. M. Gutiérrez-Zorrilla, *Inorg. Chem.* **2006**, *45*, 108; b) S. Reinoso, P. Vitoria, L. S. Felices, L. Lezama, J. M. Gutiérrez-Zorrilla, *Chem. Eur. J.* **2005**, *11*, 1538; c) L. S. Felices, P. Vitoria, J. M. Gutiérrez-Zorrilla, L. Lezama, S. Reinoso, *Inorg. Chem.* **2006**, *45*, 7748; d) Q. Zhai, X. Wu, S. Chen, Z. Zhao, C. Lu, *Inorg. Chem.* **2007**, *46*, 5046.
[35] N. Zamstein, A. Tarantul, B. Tsukerblat, *Inorg. Chem.* **2007**, *46*, 8851.
[36] H. Oshio, Y. Saito, T. Ito, *Angew. Chem.* **1997**, *109*, 2789; *Angew. Chem. Int. Ed. Engl.* **1997**, *36*, 2673.
[37] a) J. J. Borrás-Almenar, J. M. Clemente-Juan, E. Coronado, B. S. Tsukerblat, *Inorg. Chem.* **1999**, *38*, 6081; b) J. J. Borrás-Almenar, J. M. Clemente-Juan, E. Coronado, B. S. Tsukerblat, *J. Comput. Chem.* **2001**, *22*, 985.
[38] O. Kahn, *Molecular Magnetism*, VCH, New York, **1993**.
[39] B. E. Myers, L. Berger, S. A. Friedberg, *J. Appl. Phys.* **1968**, *40*, 1149.
[40] a) V. H. Crawford, H. V. Richardson, J. R. Wason, D. J. Hodgson, W. E. Hatfield, *Inorg. Chem.* **1976**, *15*, 2107; b) L. Merz, W. Haase, *J. Chem. Soc. Dalton Trans.* **1980**, 875; c) M. Handa, N. Koga, S. Kida, *Bull. Chem. Soc. Jpn.* **1988**, *61*, 3853; d) E. Ruiz, P. Alemany, S. Alvarez, J. Cano, *J. Am. Chem. Soc.* **1997**, *119*, 1297; e) G. Aromí, J. Ribas, P. Gamez, O. Roubeau, H. Kooijman, A. L. Spek, S. Teat, E. MacLean, H. Stoeckli-Evans, J. Reedijk, *Chem. Eur. J.* **2004**, *10*, 6476; f) M. P. Shores, B. M. Bartlett, D. G. Nocera, *J. Am. Chem. Soc.* **2005**, *127*, 17986.
[41] a) G. M. Sheldrick, *SHELXS97*, *Program for Crystal Structure Solution*; University of Göttingen: Göttingen, Germany, **1997**; b) G. M. Sheldrick, *SHELXL97*, *Progra*m *for Crystal Structure Refinement*; University of Göttingen: Göttingen, Germany, **1997**.

Received: May 6, 2008
Published online: August 21, 2008

